

Decays of B , B_s and B_c to D -wave heavy-light mesons

Qiang Li, Tianhong Wang*, Yue Jiang, Han Yuan, Tian Zhou, Guo-Li Wang

Harbin Institute of Technology, Harbin, 150001, P. R. China

Abstract

We study the weak decays of $\bar{B}_{(s)}$ and B_c into D -wave heavy-light mesons, including $J^P = 2^-$ ($D_{(s)2}, D'_{(s)2}, B_{(s)2}, B'_{(s)2}$) and 3^- ($D_{(s)3}^*, B_{(s)3}^*$) states. The weak decay hadronic matrix elements are achieved based on the instantaneous Bethe-Salpeter method. The branching ratios for \bar{B} decays are $\mathcal{B}[\bar{B} \rightarrow D_2 e \bar{\nu}_e] = 1.1 \times 10^{-3}$, $\mathcal{B}[\bar{B} \rightarrow D_2' e \bar{\nu}_e] = 4.1 \times 10^{-4}$, and $\mathcal{B}[\bar{B} \rightarrow D_3^* e \bar{\nu}_e] = 1.0 \times 10^{-3}$, respectively. For semi-electronic decays of \bar{B}_s to $D_{s2}, D_{s2}',$ and D_{s3}^* , the corresponding branching ratios are 1.7×10^{-3} , 5.2×10^{-4} , and 1.5×10^{-3} , respectively. The branching ratios of semi-electronic decays of B_c to D -wave D mesons are in the order of 10^{-5} . We also achieved the forward-backward asymmetry, angular spectra, and lepton momentum spectra. In particular the distribution of decay widths for 2^- states D_2 and D_2' varying along with mixing angle are presented.

1. Introduction

The D -wave $D_{(s)}$ mesons have attracted lots of attention since numerous excited charmed states are discovered by BaBar [1], and LHCb [2–5]. In 2010 BaBar observed four signals $D(2550)^0$, $D^*(2600)^0$, $D(2750)^0$, and $D^*(2760)^0$ for the first time [1], where the last two are expected to lie in the mass region of four D -wave charm mesons [6]. Later the LHCb reported two natural parity resonances $D_J^*(2650)^0$ and $D_J^*(2760)^0$ in the $D^{*+}\pi^-$ mass spectrum and measured their angular distribution [2]. The same final states also show the presence of two unnatural parity states, $D_J(2580)^0$ and $D_J(2740)^0$. Here the natural parity denotes states with $J^P = 0^+, 1^-, 2^+, 3^-, \dots$ with $P = (-1)^J$, while the unnatural parity indicates series with $J^P = 0^-, 1^+, 2^-, \dots$.

Then in May 2015, LHCb confirmed that the $D_J^*(2760)^0$ resonance has spin 1 [4]. The mass and width are measured as $m[D_1^*(2760)^0] = 2781 \pm 22$ MeV and $\Gamma[D_1^*(2760)^0] = 177 \pm 38$ MeV, where we have combined the statistical and systematic uncertainties in quadrature for simplicity. Later LHCb determined $D_J^*(2760)^-$ to have spin-parity 3^- and it is interpreted as $D_3^*(2760)^-$, namely the 3D_3 $\bar{c}d$ state. The mass and width are measured as $m[D_3^*(2760)] = 2798 \pm 10$ MeV and $\Gamma[D_3^*(2760)] = 105 \pm 30$ MeV [5].

For the D -wave charm-strange meson, BaBar first observed the $D_{sJ}^*(2860)$ [7, 8]. And then LHCb's results support that $D_{sJ}^*(2860)$ is an admixture of the spin-1 and spin-3 [9, 10]. The measured mass and width for D_{s3}^* are 2861 ± 7 and 53 ± 10 MeV, respectively. The two D -wave charm-strange mesons with $J = 2$, namely the 2^- states D_{s2} and D_{s2}' are still undiscovered in experiment.

Identification of these new excited charmed mesons can be found in Refs. [11–19]. We will follow Godfrey's assignments on D -wave $D_{(s)J}^{(*)}$ mesons in Ref. [19], where $D_{s3}^*(2860)$ is identified as 1^3D_3 $c\bar{s}$; $D_3^*(2798)^0$ is identified as 1^3D_3 ($c\bar{q}$) state; $D_1^*(2760)^0$ is interpreted as 1^3D_1 ($c\bar{q}$); and the $D_J(2750)^0$ reported by BaBar and $D_J(2740)^0$ reported by LHCb are identified as the same state with $1D_2$ ($c\bar{q}$), where q denotes a light quark u or d .

These D -wave excited states still need more experimental data to be discovered or confirmed. The identification and spin-parity assignments in above literature are just tentative. As the LHC

*Corresponding author

Email addresses: lrhit@protonmail.com (Qiang Li), thwang@hit.edu.cn (Tianhong Wang), jiangure@hit.edu.cn (Yue Jiang), hanyuan@hit.edu.cn (Han Yuan), tianzhou@hit.edu.cn (Tian Zhou), gl_wang@hit.edu.cn (Guo-Li Wang)

accumulates more and more data, the study of these D -wave charm and charm-strange mesons in the weak decay of $B_{(s)}$ and B_c meson becomes necessary and important. The properties of $D_{(s)J}^{(*)}$ in $B_{(s)}$ and B_c decays would be helpful in identification of these excited $D_{(s)}$ mesons. The semi-leptonic decays of $B_{(s)}$ into D -wave charmed mesons have been studied by QCD sum rules [20–22] and constituent quark models in the framework of heavy quark effective theory (HQET) [23, 24]. Most of previous work is based on the HQET. The systematic studies on weak decays of $\bar{B}_{(s)}$ into D -wave $D_{(s)2}$, $D'_{(s)2}$ and $D_{(s)3}^*$ are still quite less while all these D -wave charmed mesons are hopefully to be detected in the near future experiments. On the other hand, in 2012 the BaBar Collaboration reported the ratio of $\mathcal{B}(\bar{B} \rightarrow D^{(*)} \tau^- \bar{\nu}_\tau)$ relative to $\mathcal{B}(\bar{B} \rightarrow D^{(*)} e^- \bar{\nu}_e)$, which exceed the standard model expectation by 2σ (2.7σ) [25] and may hint the new physics. So it is quite necessary to investigate this ratio for $\bar{B}_{(s)}$ and B_c decays into higher excited $D_{(s)}$ mesons.

In this work we will concentrate on the semi-leptonic and non-leptonic decays of \bar{B} (\bar{B}_s, B_c) into D -wave D (D_s) meson, including 2^- ($D_{(s)2}, D'_{(s)2}$) and 3^- ($D_{(s)3}^*$) states. For completeness, the weak decays of B_c to D -wave bottomed mesons are also studied. We use the Instantaneous Bethe-Salpeter equation (IBS) [26] to get the hadronic transition form factors. BS equation [27] is the relativistic two-body bound states formula. Based on our previous studies [28–31], the relativistic corrections for transitions of higher excited states are larger and more important than that for the ground states, so the relativistic method is more reliable for the processes involved the high excited states. In the instantaneous approximation of the interaction kernel, we can achieve the Salpeter equation. The Salpeter method has been widely used to deal with heavy mesons' decay constants calculation [32, 33], annihilation rate [34, 35], and hadronic transition [28–31].

This paper is organized as follows: first we present the general formalism of semi-leptonic and non-leptonic decay for $\bar{B}_{(s)}$ meson, including decay width, forward-backward asymmetry, and lepton spectra. In Section 3 we compute the form factors in hadronic transition by Salpeter method. In Section 4 we give the numerical results and discussions. Finally we give a short summary of this work.

2. Formalism of semi-leptonic and non-leptonic decays

In this section, firstly we will derive the formalism of transition amplitudes for $\bar{B}_{(s)}$ to D -wave heavy-light mesons. Then the formalisms of interested observables are presented. We will take the $\bar{B} \rightarrow D_J^{(*)}$ transition as an example to show the calculation details, while results for transition of B_s and B_c will be given directly.

2.1. Semi-leptonic decay amplitude

The Feynman diagram responsible for \bar{B} semi-leptonic decay is showed in Fig. 1, where we use P and P_F to denote the momenta of \bar{B} and $D_J^{(*)}$ respectively. The transition amplitude \mathcal{A} for the

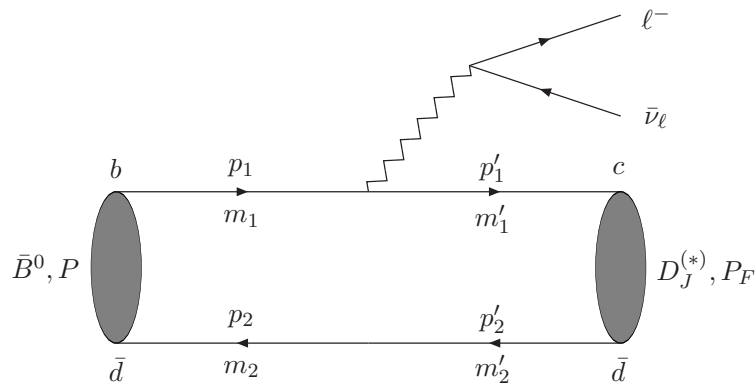


Fig. 1: Feynman diagram for semi-leptonic decay of \bar{B} to $D_J^{(*)}$ ($J = 2, 3$). $m_i(m'_i)$ and $p_i(p'_i)$ are the constituent quark mass and momentum for initial (final) state, respectively.

process $\bar{B} \rightarrow D_J^{(*)} \ell \bar{\nu}$ can be written directly as

$$\mathcal{A} = \frac{G_F}{\sqrt{2}} V_{cb} l^\mu \langle D_J^{(*)} | J_\mu | \bar{B} \rangle. \quad (1)$$

In above equation, G_F denotes the Fermi weak coupling constant; V_{cb} is the Cabibbo-Kobayashi-Maskawa matrix element; the lepton matrix element l^μ reads

$$l^\mu = \bar{u}(p_\ell) \Gamma^\mu v(p_\nu), \quad (2)$$

where ℓ ($\bar{\nu}_\ell$) denotes the charged lepton (anti-neutrino), and $p_\ell(p_\nu)$ denotes the corresponding momentum, and the definition $\Gamma^\mu = \gamma^\mu(1 - \gamma^5)$ is used; $\langle D_J^{(*)} | J_\mu | \bar{B} \rangle$ is the hadronic transition element, where $J_\mu = \bar{c} \Gamma_\mu b$ is the weak current.

We use \mathcal{M}^μ to denote hadronic transition element $\langle D_J^{(*)} | J^\mu | \bar{B} \rangle$, which can be described with form factors. The general form of the hadronic matrix element depends on the total angular momentum J of the final meson. For D_2 (D_2') and D_3^* the form factors are defined as

$$\mathcal{M}^\mu = \begin{cases} e_{\alpha\beta} P^\alpha (s_1 P^\beta P^\mu + s_2 P^\beta P_F^\mu + s_3 g^{\beta\mu} + i s_4 \epsilon^{\mu\beta P P_F}) & \text{if } J = 2, \\ e_{\alpha\beta\gamma} P^\alpha P^\beta (h_1 P^\gamma P^\mu + h_2 P^\gamma P_F^\mu + h_3 g^{\gamma\mu} + i h_4 \epsilon^{\mu\gamma P P_F}) & \text{if } J = 3. \end{cases} \quad (3)$$

In above equation, we used the definition $\epsilon_{\mu\nu P P_F} = \epsilon_{\mu\nu\alpha\beta} P^\alpha P_F^\beta$ where $\epsilon_{\mu\nu\alpha\beta}$ is the totally antisymmetric Levi-Civita tensor; $g^{\mu\nu}$ is the Minkowski metric tensor; $e_{\alpha\beta}$ and $e_{\alpha\beta\gamma}$ are the polarization tensor for $J = 2$ and 3 mesons, respectively, which are completely symmetric; s_i and h_i ($i = 1, 2, 3, 4$) are the form factors for $J = 2$ and 3, respectively. To state it more clearly, we will use s_i , t_i , and h_i to denote the form factors for transitions \bar{B} to D_2 , D_2' , and D_3^* , respectively. S_i , T_i , and H_i are used to represent the form factors of B_c^- to \bar{D}_2 , D_2' , and D_3^* , respectively. The definition forms are the same with that for transition $\bar{B} \rightarrow D_J^{(*)}$, just s_i is replaced by S_i , t_i by T_i , and h_i by H_i . For \bar{B}_s decays, the corresponding form factor behaviors are very similar to \bar{B} decays. The detailed calculations of these form factors will be given in next section.

After summing the polarization of all the final states, including the charged lepton, anti-neutrino and the final $D_J^{(*)}$, we obtain

$$|\overline{\mathcal{A}}|^2 = \frac{G_F^2}{2} |V_{cb}|^2 L^{\mu\nu} H_{\mu\nu}, \quad (4)$$

where the lepton tensor $L^{\mu\nu}$ has the following form

$$L^{\mu\nu} = 8(p_\ell^\mu p_\nu^\nu + p_\nu^\mu p_\ell^\nu - p_\ell \cdot p_\nu g^{\mu\nu} - i \epsilon^{\mu\nu p_\ell p_\nu}). \quad (5)$$

$H_{\mu\nu}$ is the hadronic tensor describing the propagator-meson interaction vertex, which depends on P , P_F and the corresponding form factors. It can be written as

$$H_{\mu\nu} = \sum_{s=-J}^J \mathcal{M}_\mu^{(s)} \mathcal{M}_\nu^{*(s)} = N_1 P_\mu P_\nu + N_2 (P_\mu P_{F\nu} + P_\nu P_{F\mu}) + N_4 P_{F\mu} P_{F\nu} + N_5 g_{\mu\nu} + i N_6 \epsilon_{\mu\nu P P_F}, \quad (6)$$

where the summation is over the polarization of final $D_J^{(*)}$ meson; N_i is related to the form factors s_i for D_2 , t_i for D_2' or h_i for D_3^* . The detailed expressions for N_i can be found in appendix A.

2.2. Non-leptonic decay amplitude

The Feynman diagram for the non-leptonic decay of \bar{B} to $D_J^{(*)}$ and a light meson X is showed in Fig. 2. As a preliminary study for non-leptonic decays of \bar{B} to D -wave D mesons, we will work in the framework of naive factorization approximation [36, 37], which has been widely used in heavy mesons' weak decays [38–41]. The factorization assumption is expected to hold for process that involves a heavy meson and a light meson, provided the light meson is energetic [42]. Also we only consider

the processes when the light meson X is π , ρ , K , or K^* . In the naive factorization approximation,

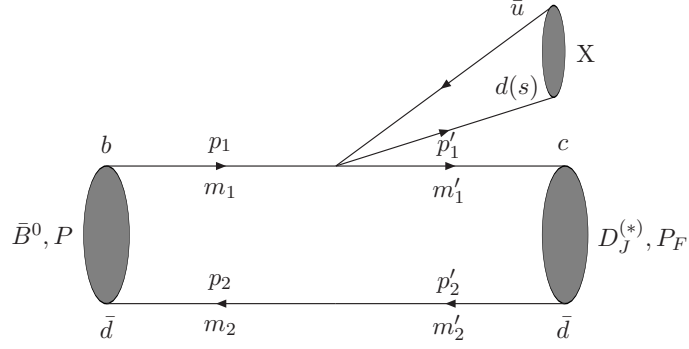


Fig. 2: The Feynman diagram of the nonleptonic decay of $\bar{B}_{(s)}$ meson into D -wave charmed meson. X denotes a light meson.

the decay amplitude can be factorized as the product of two parts, the hadronic transition matrix element and an annihilation matrix element. Then we can write the non-leptonic decay amplitude as

$$\mathcal{A}[\bar{B} \rightarrow D_J^{(*)} X] \simeq \frac{G_F}{\sqrt{2}} V_{cb} V_{uq} a_1(\mu) \langle D_J^{(*)} | J_\mu | \bar{B} \rangle \langle X | (\bar{q}u)_{V-A} | 0 \rangle, \quad (7)$$

where we have used the definition $(\bar{q}u)_{V-A} = \bar{q}\Gamma^\mu u$ and q denotes a d or s quark field; V_{uq} denotes the corresponding CKM matrix element; $a_1 = c_1 + \frac{1}{N_c}c_2$, where $N_c = 3$ is the number of colors. For b decays, we take $\mu = m_b$, and $a_1 = 1.14$, $a_2 = -0.2$ [39] are used in this work. The annihilation matrix element can be expressed by decay constant as

$$\langle X | (\bar{q}u)_{V-A} | 0 \rangle = \begin{cases} i P_X^\mu f_P & X \text{ is a pseudoscalar meson } (\pi, K), \\ e^\mu M_X f_V & X \text{ is a vector meson } (\rho, K^*). \end{cases} \quad (8)$$

M_X , P_X are the mass and momentum of X meson, respectively; the meson polarization vector e^μ satisfies $e_\mu P_X^\mu = 0$ and the completeness relation is given by $\sum_s e_{(s)}^\mu e_{(s)}^\nu = \frac{P_X^\mu P_X^\nu}{M_X^2} - g^{\mu\nu}$, where s denotes the polarization state; f_P and f_V are the corresponding decay constants.

Then the $|\overline{\mathcal{A}}|^2$ can be expressed by hadronic tensor $H_{\mu\nu}$, which is just the same with that in the corresponding semi-leptonic decays, and light meson tensor $X^{\mu\nu}$ as

$$|\overline{\mathcal{A}}|^2 = \frac{G_F^2}{2} |V_{cb}|^2 |V_{uq}|^2 a_1^2 H_{\mu\nu} X^{\mu\nu}, \quad (9)$$

where $X^{\mu\nu}$ has the following expression

$$X^{\mu\nu} = \langle X | (\bar{q}\Gamma^\mu u) | 0 \rangle \langle X | \bar{q}\Gamma^\nu u | 0 \rangle^* = \begin{cases} P_X^\mu P_X^\nu f_P^2 & X \text{ is a pseudoscalar meson,} \\ (P_X^\mu P_X^\nu - M_X^2 g^{\mu\nu}) f_V^2 & X \text{ is a vector meson.} \end{cases} \quad (10)$$

2.3. Several observables

One of the interested quantity in \bar{B} semi-leptonic decay is the angular distribution of the decay width Γ , which can be described as

$$\frac{d\Gamma}{d\cos\theta} = \int \frac{1}{(2\pi)^3} \frac{|\mathbf{p}_\ell^*| |\mathbf{p}_F^*|}{16M^3} |\overline{\mathcal{A}}|^2 dm_{\ell\nu}^2, \quad (11)$$

where M is the initial \bar{B} mass; $m_{\ell\nu}^2 = (p_\ell + p_\nu)^2$ is the invariant mass square of ℓ and $\bar{\nu}$; \mathbf{p}_ℓ^* and \mathbf{p}_F^* are the three momenta of ℓ and $D_J^{(*)}$ in the $\ell\bar{\nu}$ rest frame, respectively; θ is the angle between \mathbf{p}_ℓ^* and \mathbf{p}_F^* ; $|\mathbf{p}_\ell^*| = \frac{1}{2m_{\ell\nu}} \lambda^{\frac{1}{2}}(m_{\ell\nu}^2, M_\ell^2, M_\nu^2)$ and $|\mathbf{p}_F^*| = \frac{1}{2m_{\ell\nu}} \lambda^{\frac{1}{2}}(m_{\ell\nu}^2, M^2, M_F^2)$, where we have used the Källén function $\lambda(a, b, c) = (a^2 + b^2 + c^2 - 2ab - 2bc - 2ac)$, M_ℓ and M_ν are the lepton mass and anti-neutrino

mass, respectively. Another quantity we are interested is the forward-backward asymmetry A_{FB} , which is defined as

$$A_{FB} = \frac{\Gamma_{\cos\theta>0} - \Gamma_{\cos\theta<0}}{\Gamma_{\cos\theta>0} + \Gamma_{\cos\theta<0}}. \quad (12)$$

The decay width varying along with charged lepton 3-momentum $|\mathbf{p}_\ell|$ is given by

$$\frac{d\Gamma}{d|\mathbf{p}_\ell|} = \int \frac{1}{(2\pi)^3} \frac{|\mathbf{p}_\ell|}{16M^2 E_\ell} |\overline{\mathcal{A}}|^2 dm_{\ell\nu}^2, \quad (13)$$

where E_ℓ denotes the charged lepton energy in the rest frame of initial state meson.

The non-leptonic decay width of the \bar{B} meson is given by

$$\Gamma = \frac{|\mathbf{p}|}{8\pi M^2} |\overline{\mathcal{A}}|^2, \quad (14)$$

where \mathbf{p} represents the 3-momentum of the final $D_J^{(*)}$ in \bar{B} rest frame, which is expressed as $|\mathbf{p}| = \frac{1}{2M} \lambda^{\frac{1}{2}}(M^2, M_X^2, M_F^2)$.

3. Hadronic transition matrix element

The hadronic transition matrix element $\langle D_J^{(*)} | J^\mu | \bar{B} \rangle$ plays an key role in the calculations of \bar{B} semi-leptonic and non-leptonic decays. In this section we will give details to calculate the hadronic transition matrix element by Bethe-Salpeter method in the framework of constituent quark model.

3.1. Formalism of hadronic transition matrix element with Bethe-Salpeter method

According to the Mandelstam formalism [43], the hadronic transition amplitude \mathcal{M}^μ can be written by Beter-Salpeter (BS) wave function as

$$\mathcal{M}^\mu = -i \int \frac{d^4 q d^4 q'}{(2\pi)^4} \text{Tr} [\bar{\Psi}_D(q', P_F) \Gamma^\mu \Psi_B(q, P) (m_2 + \not{p}_2) \delta^4(p_2 - p'_2)], \quad (15)$$

where $\Psi_B(q, P)$ and $\Psi_D(q', P_F)$ are the BS wave functions of the \bar{B} meson and the final $D_J^{(*)}$, respectively; $\bar{\Psi}$ is defined as $\gamma^0 \Psi^\dagger \gamma^0$; q and q' are respectively the inner relative momenta of \bar{B} and $D_J^{(*)}$ system, which are related to the quark (anti-quark) momentum $p_1^{(i)}$ ($p_2^{(i)}$) by $p_i = \alpha_i P + (-1)^{(i+1)} q$ and $p'_i = \alpha'_i P_F + (-1)^{(i+1)} q'$ ($i = 1, 2$). And here we defined the symbols $\alpha_i = \frac{m_i}{m_1 + m_2}$ and $\alpha'_i = \frac{m'_i}{m'_1 + m'_2}$, where m_i and m'_i are masses of the constituent quarks in the initial and final bound states, respectively (see Fig. 1). Here in \bar{B} decays we have $m_1 = m_b$, $m'_1 = m_c$, $m_2 = m'_2 = m_d$. As there is a delta function in above equation, the relative momenta q and q' are related by $q' = q - (\alpha_2 P - \alpha'_2 P_F)$.

In the instantaneous approximation [26], the inner interaction kernel between quark and anti-quark in bound state is independent of the time component $q_P (= q \cdot P)$ of q . By performing the contour integral on q_P and then we can express the hadronic transition amplitude as [31]

$$\mathcal{M}^\mu = \int \frac{d^3 q_\perp}{(2\pi)^3} \text{Tr} \left[\frac{\not{P}}{M} \bar{\psi}_D(q'_\perp) \Gamma^\mu \psi_B(q_\perp) \right], \quad (16)$$

where we have used the definitions $q_\perp \equiv q - \frac{P \cdot q}{M^2} P$ and $q'_\perp \equiv q' - \frac{P \cdot q'}{M^2} P$. Here ψ denotes the 3-dimensional positive Salpeter wave function (see appendix B). ψ_B and ψ_D denote the positive Salpeter wave functions for \bar{B} and $D_J^{(*)}$, respectively, and $\bar{\psi}_D$ is defined $\gamma^0 \psi_D^\dagger \gamma^0$.

The positive Salpeter wave function for $^1S_0(0^-)$ state can be written as [44]

$$\psi_B(^1S_0) = \left[A_1 + A_2 \frac{\not{P}}{M} + A_3 \frac{\not{q}_\perp}{M} + A_4 \frac{\not{P} \not{q}_\perp}{M^2} \right] \gamma^5, \quad (17)$$

where we have

$$\begin{aligned} A_1 &= \frac{M}{2} \left[\frac{\omega_1 + \omega_2}{m_1 + m_2} k_1 + k_2 \right], & A_3 &= -\frac{M(\omega_1 - \omega_2)}{m_1\omega_2 + m_2\omega_1} A_1, \\ A_2 &= \frac{M}{2} \left[k_1 + \frac{m_1 + m_2}{\omega_1 + \omega_2} k_2 \right], & A_4 &= -\frac{M(m_1 + m_2)}{m_1\omega_2 + m_2\omega_1} A_1. \end{aligned} \quad (18)$$

So there are only two undetermined wave function k_1 and k_2 here, which are the functions of q_\perp . The positive Salpeter wave function for $3^-(^3D_3)$ state with unequal mass of quark and anti-quark has the following forms [45]

$$\begin{aligned} \psi_D(^3D_3) &= e_{\mu\nu\alpha} q_\perp^\nu q_\perp^\alpha \left[q_\perp'^\mu (n_1 + n_2 \frac{\not{P}_F}{M_F} + n_3 \frac{\not{q}'_\perp}{M_F} + n_4 \frac{\not{P}_F \not{q}'_\perp}{M_F^2}) + \gamma^\mu (n_5 M_F + n_6 \not{P}_F) \right. \\ &\quad \left. + n_7 (\gamma^\mu \not{q}' - q'^\mu) + n_8 \frac{(\gamma^\mu \not{P}_F \not{q}'_\perp + \not{P}_F q_\perp'^\mu)}{M_F} \right]. \end{aligned} \quad (19)$$

In above equation n_i ($i = 1, 2, \dots, 8$) can be expressed with 4 wave functions u_i ($i = 3, 4, 5, 6$) as below,

$$\begin{aligned} n_1 &= \frac{[(\omega'_1 + \omega'_2)(q_\perp'^2 u_3 + M_F^2 u_5) + (m'_1 + m'_2)(q_\perp'^2 u_4 - M_F^2 u_6)]}{2M_F(m'_1\omega'_2 + m'_2\omega'_1)}, \\ n_2 &= \frac{[(m'_1 - m'_2)(q_\perp'^2 u_3 + M_F^2 u_5) + (\omega'_1 - \omega'_2)(q_\perp'^2 u_4 - M_F^2 u_6)]}{2M_F(m'_1\omega'_2 + m'_2\omega'_1)}, \\ n_3 &= \frac{1}{2} \left[u_3 + \frac{m'_2 + m'_2}{\omega'_1 + \omega'_2} u_4 - \frac{2M_F^2}{m'_1\omega'_2 + m'_2\omega'_1} u_6 \right], \\ n_4 &= \frac{1}{2} \left[u_4 + \frac{\omega'_1 + \omega'_2}{m'_1 + m'_2} u_3 - \frac{2M_F^2}{m'_1\omega'_2 + m'_2\omega'_1} u_5 \right], \\ n_5 &= \frac{1}{2} \left[u_5 - \frac{\omega'_1 + \omega'_2}{m'_1 + m'_2} u_6 \right], & n_6 &= \frac{1}{2} \left[u_6 - \frac{m'_1 + m'_2}{\omega'_1 + \omega'_2} u_5 \right], \\ n_7 &= \frac{M_F(\omega'_1 - \omega'_2)}{(m'_1\omega'_2 + m'_2\omega'_1)} n_5, & n_8 &= \frac{M_F(\omega'_1 + \omega'_2)}{(m'_1\omega'_2 + m'_2\omega'_1)} n_6. \end{aligned} \quad (20)$$

In above Salpeter positive wave functions ψ_B and ψ_D , the undetermined wave functions k_1, k_2 for 0^- and u_i ($i = 3, 4, 5, 6$) for 3^- can be achieved by solving the full Salpeter equations numerically (see appendix B). The positive Salpeter wave functions for 1D_2 [35], and 3D_2 [45] states can be seen in appendix C. $e^{\mu\nu\alpha}$ is the symmetric polarization tensor for spin-3 and satisfies the following relations [46]

$$e^{\mu\nu\alpha} g_{\mu\nu} = 0, \quad e^{\mu\nu\alpha} P_{F\mu} = 0, \quad (21)$$

$$\sum_s e_{(s)}^{abc} e_{(s)}^{\mu\nu\alpha} = \frac{1}{6} \Omega_1^{abc;\mu\nu\alpha} - \frac{1}{15} \Omega_2^{abc;\mu\nu\alpha}, \quad (22)$$

where

$$\begin{aligned} \Omega_1^{abc;\mu\nu\alpha} &= g_\perp^{a\mu} g_\perp^{b\nu} g_\perp^{c\alpha} + g_\perp^{a\mu} g_\perp^{b\alpha} g_\perp^{c\nu} + g_\perp^{a\nu} g_\perp^{b\mu} g_\perp^{c\alpha} + g_\perp^{a\nu} g_\perp^{b\alpha} g_\perp^{c\mu} + g_\perp^{a\alpha} g_\perp^{b\mu} g_\perp^{c\nu} + g_\perp^{a\alpha} g_\perp^{b\nu} g_\perp^{c\mu}, \\ \Omega_2^{abc;\mu\nu\alpha} &= g_\perp^{ab} g_\perp^{c\mu} g_\perp^{\nu\alpha} + g_\perp^{ab} g_\perp^{c\nu} g_\perp^{\mu\alpha} + g_\perp^{ab} g_\perp^{c\alpha} g_\perp^{\mu\nu} + g_\perp^{ac} g_\perp^{b\mu} g_\perp^{\nu\alpha} + g_\perp^{ac} g_\perp^{b\nu} g_\perp^{\mu\alpha} + g_\perp^{ac} g_\perp^{b\alpha} g_\perp^{\mu\nu} \\ &\quad + g_\perp^{bc} g_\perp^{a\mu} g_\perp^{\nu\alpha} + g_\perp^{bc} g_\perp^{a\nu} g_\perp^{\mu\alpha} + g_\perp^{bc} g_\perp^{a\alpha} g_\perp^{\mu\nu}. \end{aligned} \quad (23)$$

and we have used the definition $g_\perp^{\mu\nu} = -g^{\mu\nu} + \frac{P_F^\mu P_F^\nu}{M_F^2}$.

Inserting the initial \bar{B} wave function $\psi_B(^1S_0)$ (Eq. 17) and final D_3^* wave function $\psi_D(^3D_3)$ (Eq. 19) into the hadronic transition amplitude Eq. (16), after calculating the trace and performing the integral in Eq. (16) we achieve the form factors h_i for $\bar{B} \rightarrow D_3^*$ transition defined in Eq. (3). When

performing the integral over \mathbf{q} in the rest frame of the initial meson, the following formulas are used.

$$\begin{aligned}
\int \frac{d^3\mathbf{q}}{(2\pi)^3} q_\perp^\mu &= C_1 P_{F\perp}^\mu, \\
\int \frac{d^3\mathbf{q}}{(2\pi)^3} q_\perp^\mu q_\perp^\nu &= C_{21} P_{F\perp}^\mu P_{F\perp}^\nu + C_{22} g_T^{\mu\nu}, \\
\int \frac{d^3\mathbf{q}}{(2\pi)^3} q_\perp^\mu q_\perp^\nu q_\perp^\alpha &= C_{31} P_{F\perp}^\mu P_{F\perp}^\nu P_{F\perp}^\alpha + C_{32} (g_T^{\mu\nu} P_{F\perp}^\alpha + g_T^{\mu\alpha} P_{F\perp}^\nu + g_T^{\alpha\nu} P_{F\perp}^\mu), \\
\int \frac{d^3\mathbf{q}}{(2\pi)^3} q_\perp^\mu q_\perp^\nu q_\perp^\alpha q_\perp^\beta &= C_{41} P_{F\perp}^\mu P_{F\perp}^\nu P_{F\perp}^\alpha P_{F\perp}^\beta + C_{42} (g_T^{\mu\nu} P_{F\perp}^\alpha P_{F\perp}^\beta + g_T^{\mu\alpha} P_{F\perp}^\nu P_{F\perp}^\beta + g_T^{\alpha\nu} P_{F\perp}^\mu P_{F\perp}^\beta + \\
&\quad g_T^{\alpha\beta} P_{F\perp}^\mu P_{F\perp}^\nu + g_T^{\beta\nu} P_{F\perp}^\mu P_{F\perp}^\alpha + g_T^{\beta\mu} P_{F\perp}^\nu P_{F\perp}^\alpha) + C_{43} (g_T^{\alpha\beta} g_T^{\mu\nu} + g_T^{\alpha\nu} g_T^{\mu\beta} + g_T^{\alpha\mu} g_T^{\beta\nu}),
\end{aligned}$$

where $g_T^{\mu\nu}$ are defined as $(g^{\mu\nu} - \frac{P^\mu P^\nu}{P^2})$ and $P_{F\perp}^\mu = (P_F^\mu - \frac{P_F \cdot P}{M^2} P^\mu)$. C_i is expressed as

$$\begin{cases} C_1 = |\mathbf{q}| \cos \eta, & C_{21} = \frac{1}{2} |\mathbf{q}|^2 (3 \cos^2 \eta - 1), \\ C_{22} = \frac{1}{2} |\mathbf{q}|^2 (\cos^2 \eta - 1), & C_{31} = \frac{1}{2} |\mathbf{q}|^3 (5 \cos^3 \eta - 3 \cos \eta), \\ C_{32} = \frac{1}{2} |\mathbf{q}|^3 (\cos^3 \eta - \cos \eta), & C_{41} = \frac{1}{8} |\mathbf{q}|^4 (35 \cos^4 \eta - 30 \cos^2 \eta + 3), \\ C_{42} = \frac{1}{8} |\mathbf{q}|^4 (5 \cos^4 \eta - 6 \cos^2 \eta + 1), & C_{43} = \frac{1}{8} |\mathbf{q}|^4 (\cos^4 \eta - 2 \cos^2 \eta + 1), \end{cases} \quad (24)$$

where η is the angle between \mathbf{q} and \mathbf{P}_F .

The physical 2^- D -wave states D_2 and D'_2 are the mixing states of 3D_2 and 1D_2 states, whose wave functions are what we solve directly from the full Salpeter equations. Here we will follow Ref. [47] and Ref. [48], where the mixing form for D -wave states is defined with the mixing angle α as

$$\begin{aligned}
|D_2\rangle &= +\cos \alpha |^1D_2\rangle + \sin \alpha |^3D_2\rangle, \\
|D'_2\rangle &= -\sin \alpha |^1D_2\rangle + \cos \alpha |^3D_2\rangle.
\end{aligned} \quad (25)$$

In the heavy quark limit ($m_Q \rightarrow \infty$), the D mesons are described in the $|J, j_\ell\rangle$ basis, where m_Q denotes the heavy quark mass and j_ℓ denotes the total angular momentum of the light quark. The relations between $|J, j_\ell\rangle$ and $|J, S\rangle$ for $L = 2$ are showed by

$$\begin{bmatrix} |2, 5/2\rangle \\ |2, 3/2\rangle \end{bmatrix} = \frac{1}{\sqrt{5}} \begin{bmatrix} \sqrt{2+1} & \sqrt{2} \\ -\sqrt{2} & \sqrt{2+1} \end{bmatrix} \begin{bmatrix} |^1D_2\rangle \\ |^3D_2\rangle \end{bmatrix}. \quad (26)$$

Then the mixing angle for $L = 2$ can be expressed as $\alpha = \arctan \sqrt{2/3} = 39.23^\circ$. So in this definition D_2 corresponds to the $|J^P, j_\ell\rangle = |2^-, 5/2\rangle$ state and D'_2 corresponds to the $|2^-, 3/2\rangle$ state. In this work the same mixing angle will also be used for 2^- states $D_{s2}^{(\prime)}$ and $B_{(s)2}^{(\prime)}$. Here the mixing angle is the ideal case predicted by the HEQT in the limit of $m_Q \rightarrow \infty$. The dependence for decay widths varying over the mixing angle can be seen in equations (29) and (30).

The wave functions of 1D_2 and 3D_2 states can be achieved by solving the corresponding Salpeter equations directly. Then the amplitude for physical 2^- states can be considered as the mixing of the transition amplitudes for 1D_2 and 3D_2 states, namely

$$\begin{aligned}
\mathcal{M}^\mu(D_2) &= +\cos \alpha \mathcal{M}^\mu(^1D_2) + \sin \alpha \mathcal{M}^\mu(^3D_2), \\
\mathcal{M}^\mu(D'_2) &= -\sin \alpha \mathcal{M}^\mu(^1D_2) + \cos \alpha \mathcal{M}^\mu(^3D_2).
\end{aligned} \quad (27)$$

By using Eq. (27), replacing the final state's wave function $\psi_D(^3D_3)$ by $\psi_D(^1D_2)$ and $\psi_D(^3D_2)$, and then repeating the above procedures for 3D_3 state, we can get the form factors s_i for D_2 and t_i

for D'_2 defined in Eq. (3).

3.2. Form factors

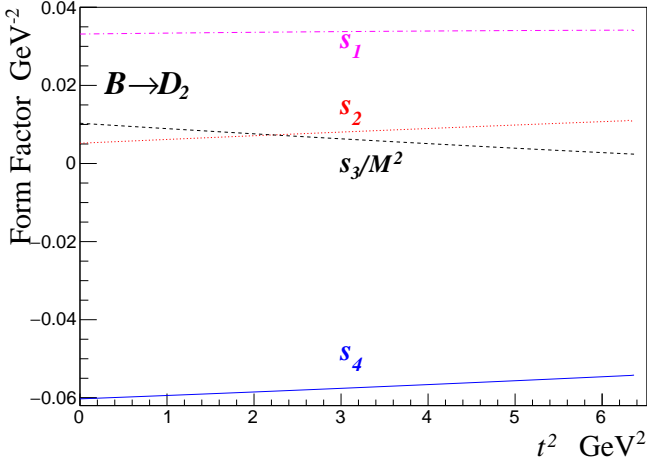
To solve the Salpeter equations, in this work we choose the Cornell potential as the inner interaction kernel as before [44], which is a linear scalar potential plus a vector interaction potential as below

$$\begin{aligned} V(\mathbf{q}) &= (2\pi)^3 V_s(\mathbf{q}) + \gamma^0 \otimes \gamma_0 (2\pi)^3 V_v(\mathbf{q}), \\ V_s(\mathbf{q}) &= -\left(\frac{\lambda}{\alpha} + V_0\right) \delta^3(\mathbf{q}) + \frac{\lambda}{\pi^2(\mathbf{q}^2 + \alpha^2)^2}, \\ V_v(\mathbf{q}) &= -\frac{2\alpha_s(\mathbf{q})}{3\pi^2(\mathbf{q}^2 + \alpha^2)}, \quad \alpha_s(\mathbf{q}) = \frac{12\pi}{27 \ln(a + \frac{\mathbf{q}^2}{\Lambda_{\text{QCD}}^2})}. \end{aligned} \quad (28)$$

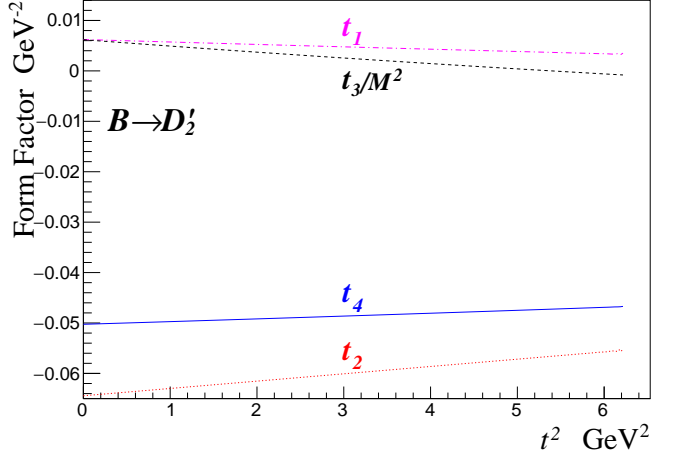
In above equations, the symbol \otimes denotes that the Salpeter wave function is sandwiched between the two γ^0 matrices. The model parameters we used are the same with before [29], which read

$$\begin{aligned} a = e &= 2.7183, & \alpha &= 0.060 \text{ GeV}, & \lambda &= 0.210 \text{ GeV}^2, \\ m_u &= 0.305 \text{ GeV}, & m_d &= 0.311 \text{ GeV}, & m_s &= 0.500 \text{ GeV}, \\ m_c &= 1.62 \text{ GeV}, & m_b &= 4.96 \text{ GeV}, & \Lambda_{\text{QCD}} &= 0.270 \text{ GeV}. \end{aligned}$$

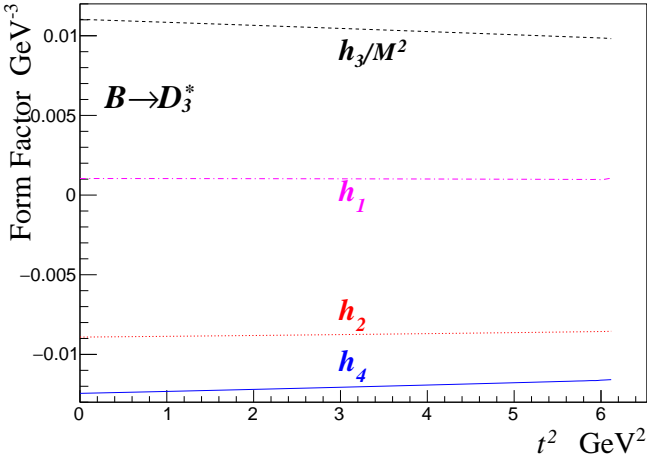
With the numerical Salpeter wave function we can obtain the form factors.



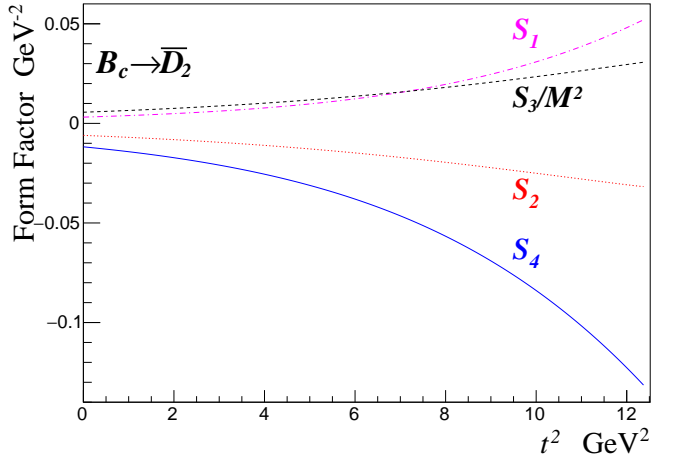
(a) Form Factors for $\bar{B} \rightarrow D_2(2^-)$.



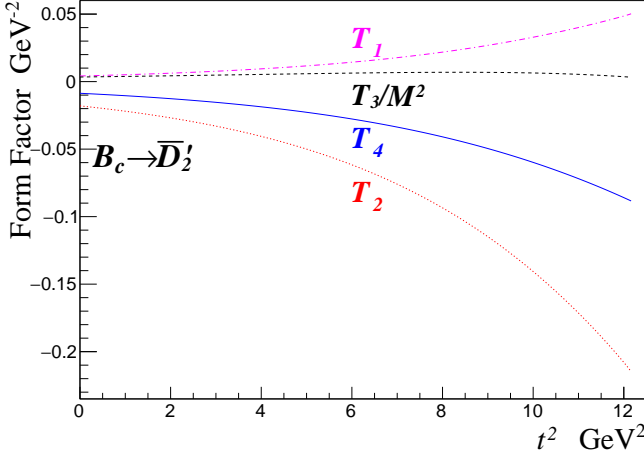
(b) Form Factors for $\bar{B} \rightarrow D'_2(2^-)$.



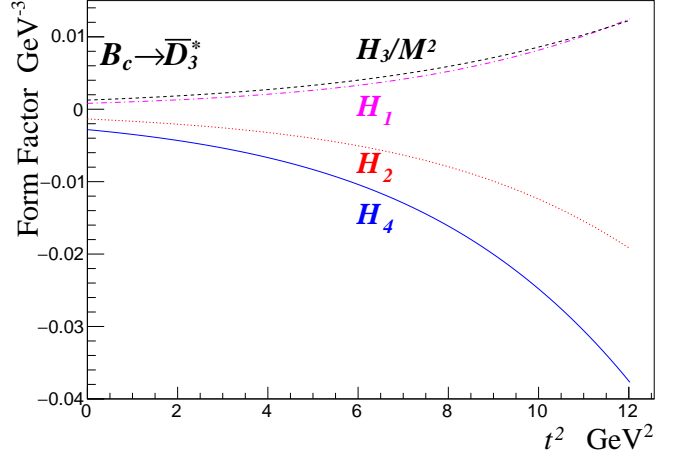
(c) Form Factors for $\bar{B} \rightarrow D_3^*(3^-)$.



(d) Form Factors for $B_c^- \rightarrow \bar{D}_2(2^-)$.



(e) Form Factors for $B_c^- \rightarrow \bar{D}_2'(2^-)$.



(f) Form Factors for $B_c^- \rightarrow \bar{D}_3^*(3^-)$.

Fig. 3: Form factors for transitions $\bar{B} \rightarrow D_J^{(*)}$ ($2^-, 3^-$) and $B_c^- \rightarrow \bar{D}_J^{(*)}$ ($2^-, 3^-$). $t^2 = (P - P_F)^2$ denotes the square of momentum transfer. To make the dimension consistent, s_3 , t_3 and h_3 are divided by M_B^2 , S_3 , T_3 and H_3 are divided by $M_{B_c}^2$.

Here we plot the $\bar{B} \rightarrow D_J^{(*)}$ form factors s_i , t_i , and h_i ($i = 1, 2, 3, 4$) changing with the square of momentum transfer $t^2 = (P - P_F)^2$ in Fig. 3(a) ~ Fig. 3(c), respectively, where s_3 , t_3 , and h_3 are divided by M_B^2 in order to keep the dimension consistent. Fig. 3(d) ~ Fig. 3(f) are the distribution of form factors S_i , T_i , and H_i for $B_c^- \rightarrow \bar{D}_J^{(*)}$ transitions. Also we divided S_3 , T_3 , and H_3 by $M_{B_c}^2$ to keep the dimension consistent. From Fig. 3, we can see that in all the range concerned the form factors are quite smooth along with t^2 . And for transitions $\bar{B} \rightarrow D_J^{(*)}$, the form factors change slowly and almost linearly when t^2 varies from 0 to $(M - M_F)^2$. For transitions $B_c^- \rightarrow \bar{D}_J^{(*)}$, the variation of form factors over t^2 is quite obvious, especially in the range with large momentum transfer.

4. Numerical Results and Discussions

Firstly we specify the meson mass, lifetime, CKM matrix elements and decay constants used in this work. For the mass of \bar{B} , \bar{B}_s , and B_c mesons we take the values from PDG [49]. We follow the mass predictions and J^P assignments of Ref. [19] for D -wave charm and charm-strange mesons. For D -wave bottom mesons B_2 , B_2' , and B_3^* we use the average values of Ref. [50] and Ref. [48]. Predictions of Ref. [48] and Ref. [51] are averaged to achieve the mass of D -wave bottom-strange mesons B_{s2} , B_{s2}' , and B_{s3}^* . These mass values we used can be seen below

$$\begin{aligned} M_B &= 5.280 \text{ GeV}, & M_{B_s} &= 5.367 \text{ GeV}, & M_{B_c} &= 6.276 \text{ GeV}, \\ M_{D_2} &= 2.750 \text{ GeV}, & M_{D_2'} &= 2.780 \text{ GeV}, & M_{D_3^*} &= 2.800 \text{ GeV}, \\ M_{D_{s2}} &= 2.846 \text{ GeV}, & M_{D_{s2}'} &= 2.872 \text{ GeV}, & M_{D_{s3}^*} &= 2.860 \text{ GeV}, \\ M_{B_2} &= 6.060 \text{ GeV}, & M_{B_2'} &= 6.100 \text{ GeV}, & M_{B_3^*} &= 6.050 \text{ GeV}, \\ M_{B_{s2}} &= 6.150 \text{ GeV}, & M_{B_{s2}'} &= 6.210 \text{ GeV}, & M_{B_{s3}^*} &= 6.190 \text{ GeV}. \end{aligned}$$

The lifetime of initial mesons we used are as below [49]

$$\tau_{\bar{B}} = 1.519 \times 10^{-12} \text{ s}, \quad \tau_{\bar{B}_s} = 1.512 \times 10^{-12} \text{ s}, \quad \tau_{B_c} = 0.452 \times 10^{-12} \text{ s}.$$

The involved CKM matrix element values are [49]

$$|V_{ud}| = 0.974, \quad |V_{us}| = 0.225, \quad |V_{ub}| = 0.0042, \quad |V_{cd}| = 0.23, \quad |V_{cs}| = 1.006, \quad |V_{cb}| = 0.041.$$

In the calculation of non-leptonic decays, the decay constants we used are [39, 49]

$$f_\pi = 130.4 \text{ MeV}, f_K = 156.2 \text{ MeV}, f_\rho = 210 \text{ MeV}, f_{K^*} = 217 \text{ MeV}.$$

4.1. Lepton spectra and A_{FB}

The distribution of \bar{B} and B_c^- decay width Γ varying along with $\cos\theta$ for e and τ modes can be seen in Fig. 4, from which we can see that, for \bar{B} decays, the distribution of semi-electronic decay widths are much more symmetric than that for the semi-taunic mode. These asymmetries over $\cos\theta$ can also be reflected by the forward-backward asymmetries A_{FB} , which are showed in Tab. I. We can see that A_{FB} is sensitive to lepton mass m_ℓ and is the monotonic function of m_ℓ . Considering the absolute values of A_{FB} , we find that for $\bar{B} \rightarrow D_J^{(*)}$ and $B_c^- \rightarrow \bar{D}_J^{(*)}$, the μ decay mode has the smallest $|A_{FB}|$.

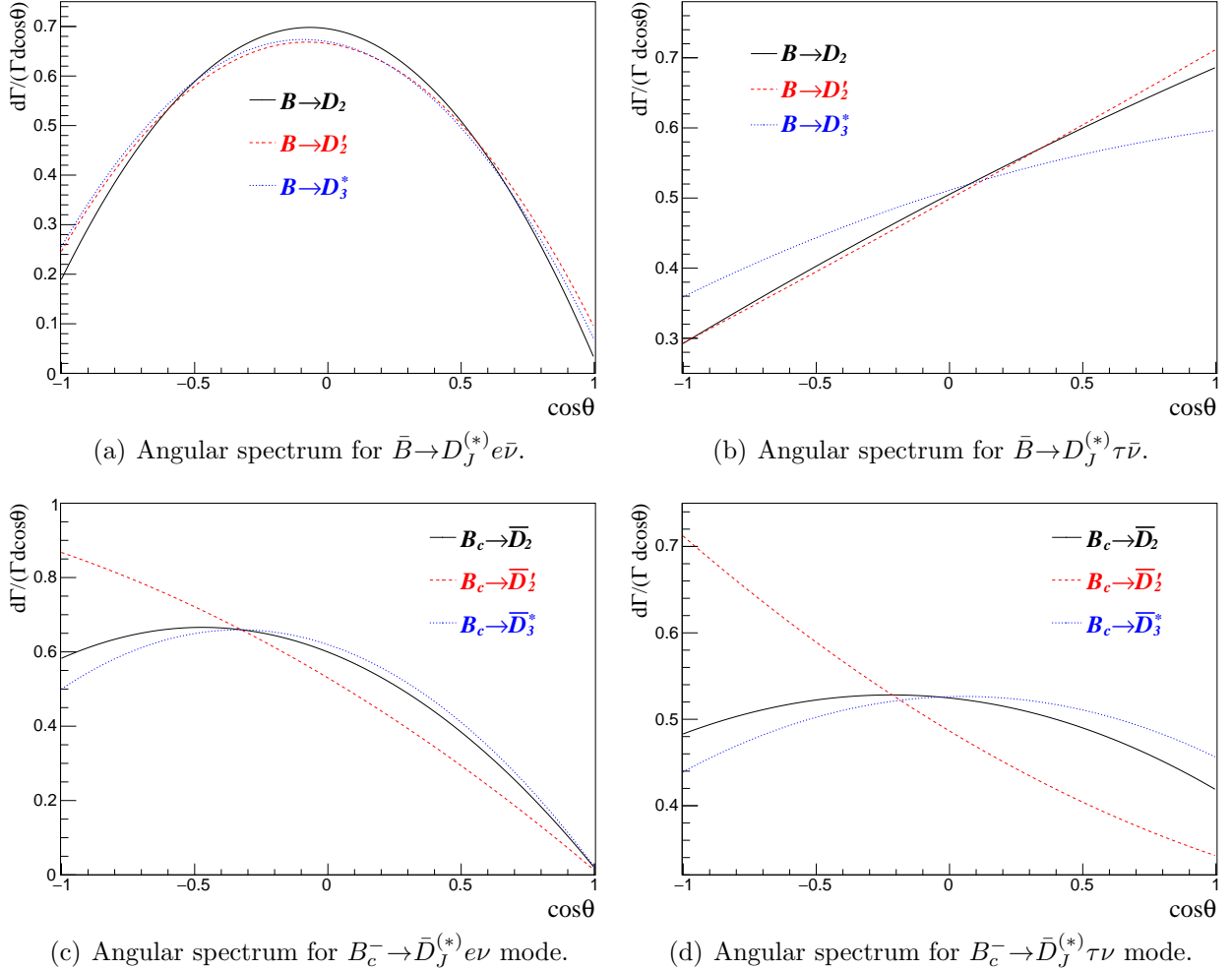
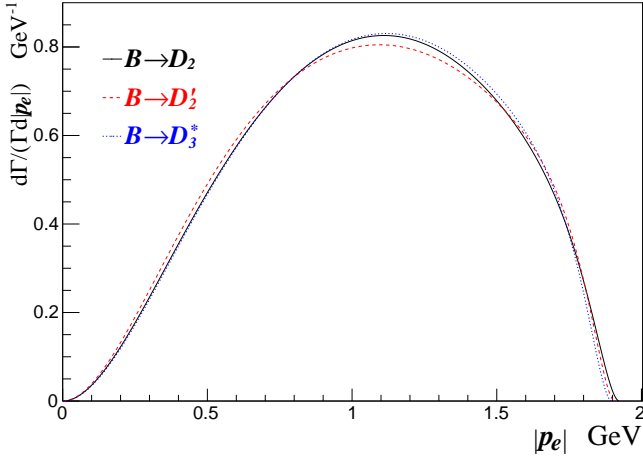


Fig. 4: The spectra of relative width vs $\cos\theta$ for semi-leptonic decays $\bar{B} \rightarrow D_J^{(*)}$ and $B_c^- \rightarrow \bar{D}_J^{(*)}$. θ is the angle between charged lepton ℓ and final charmed meson in the rest frame of $\ell\bar{\nu}$ pair.

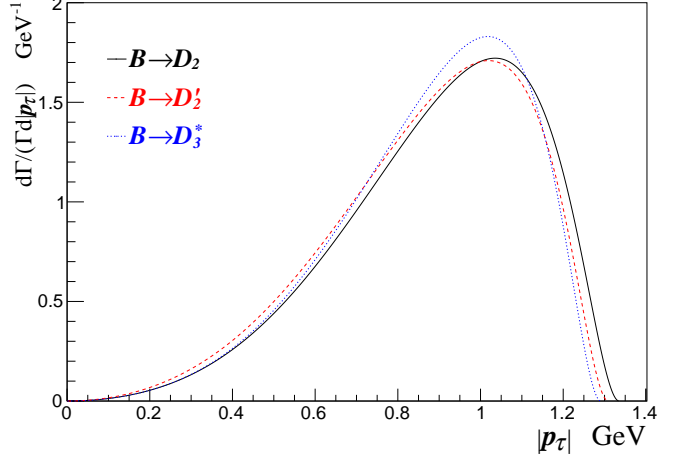
The spectra of decay widths for \bar{B} and B_c^- varying along with $|\mathbf{p}_\ell|$, the absolute value of the three-momentum for charged leptons, are showed in Fig. 5. This distribution is almost the same for \bar{B} decays into D_2 , D_2' or D_3^* . For $B_c^- \rightarrow \bar{D}_J^{(*)}$, the momentum spectrum of \bar{D}_2' is sharper than that of \bar{D}_2 and \bar{D}_3^* .

Table I: A_{FB} for semi-leptonic decays of \bar{B} , \bar{B}_s and B_c to D -wave heavy-light mesons.

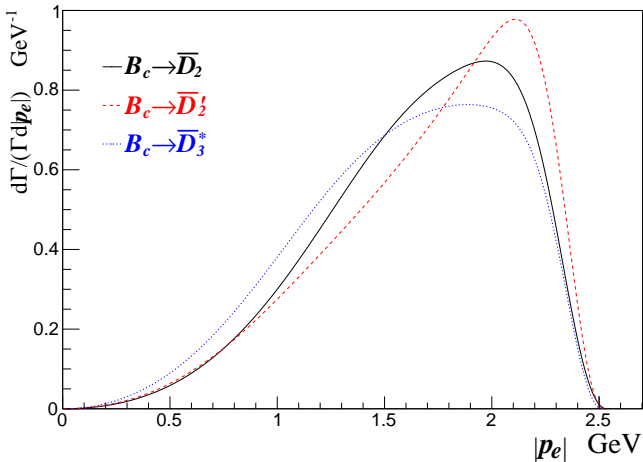
Channels	A_{FB}	Channels	A_{FB}	Channels	A_{FB}
$\bar{B} \rightarrow \bar{D}_2 e \bar{\nu}$	-0.08	$\bar{B} \rightarrow \bar{D}'_2 e \bar{\nu}$	-0.08	$\bar{B} \rightarrow \bar{D}_3^* e \bar{\nu}$	-0.10
$\bar{B} \rightarrow \bar{D}_2 \mu \bar{\nu}$	-0.05	$\bar{B} \rightarrow \bar{D}'_2 \mu \bar{\nu}$	-0.05	$\bar{B} \rightarrow \bar{D}_3^* \mu \bar{\nu}$	-0.07
$\bar{B} \rightarrow \bar{D}_2 \tau \bar{\nu}$	0.20	$\bar{B} \rightarrow \bar{D}'_2 \tau \bar{\nu}$	0.21	$\bar{B} \rightarrow \bar{D}_3^* \tau \bar{\nu}$	0.12
$\bar{B}_s \rightarrow D_{s2} e \bar{\nu}$	-0.10	$\bar{B}_s \rightarrow D'_{s2} e \bar{\nu}$	-0.09	$\bar{B}_s \rightarrow D_{s3}^* e \bar{\nu}$	-0.10
$\bar{B}_s \rightarrow D_{s2} \mu \bar{\nu}$	-0.07	$\bar{B}_s \rightarrow D'_{s2} \mu \bar{\nu}$	-0.06	$\bar{B}_s \rightarrow D_{s3}^* \mu \bar{\nu}$	-0.08
$\bar{B}_s \rightarrow D_{s2} \tau \bar{\nu}$	0.17	$\bar{B}_s \rightarrow D'_{s2} \tau \bar{\nu}$	0.20	$\bar{B}_s \rightarrow D_{s3}^* \tau \bar{\nu}$	0.11
$B_c^- \rightarrow \bar{D}_2 e \bar{\nu}$	-0.28	$B_c^- \rightarrow \bar{D}'_2 e \bar{\nu}$	-0.43	$B_c^- \rightarrow \bar{D}_3^* e \bar{\nu}$	-0.24
$B_c^- \rightarrow \bar{D}_2 \mu \bar{\nu}$	-0.28	$B_c^- \rightarrow \bar{D}'_2 \mu \bar{\nu}$	-0.42	$B_c^- \rightarrow \bar{D}_3^* \mu \bar{\nu}$	-0.23
$B_c^- \rightarrow \bar{D}_2 \tau \bar{\nu}$	-0.03	$B_c^- \rightarrow \bar{D}'_2 \tau \bar{\nu}$	-0.19	$B_c^- \rightarrow \bar{D}_3^* \tau \bar{\nu}$	-0.01
$B_c^+ \rightarrow B_2 e^+ \nu$	0.04	$B_c^+ \rightarrow B'_2 e^+ \nu$	-0.07	$B_c^+ \rightarrow B_3^* e^+ \nu$	0.03
$B_c^+ \rightarrow B_2 \mu^+ \nu$	0.23	$B_c^+ \rightarrow B'_2 \mu^+ \nu$	0.18	$B_c^+ \rightarrow B_3^* \mu^+ \nu$	0.24
$B_c^+ \rightarrow B_{s2} e^+ \nu$	0.03	$B_c^+ \rightarrow B'_{s2} e^+ \nu$	-0.03	$B_c^+ \rightarrow B_{s3}^* e^+ \nu$	0.01



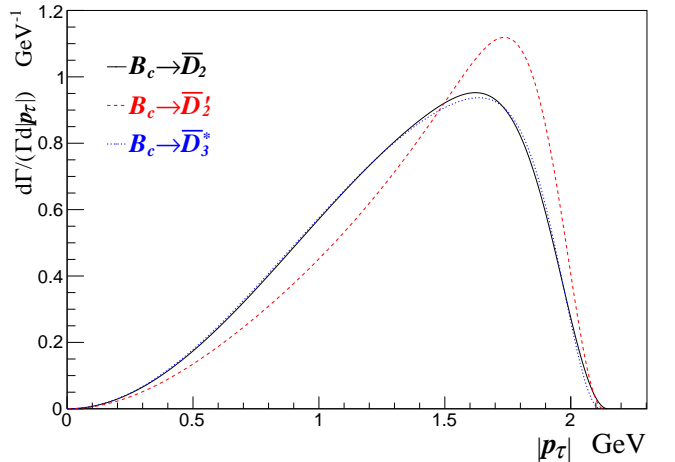
(a) Momentum spectrum for decay $\bar{B} \rightarrow D_J^{(*)} e \bar{\nu}$.



(b) Momentum spectrum for decay $\bar{B} \rightarrow D_J^{(*)} \tau \bar{\nu}$.



(c) Momentum spectrum for decay $B_c^- \rightarrow \bar{D}_J^{(*)} e \bar{\nu}$.



(d) Momentum spectrum for decay $B_c^- \rightarrow \bar{D}_J^{(*)} \tau \bar{\nu}$.

Fig. 5: The spectra of relative width vs $|\mathbf{p}_\ell|$, the absolute value of charged lepton's 3-momentum, in transitions $\bar{B} \rightarrow D_J^{(*)}$ and $B_c^- \rightarrow \bar{D}_J^{(*)}$.

4.2. Branching ratios of semi-leptonic decays

The semi-electronic decay widths we got are $\Gamma(\bar{B} \rightarrow D_2 e \bar{\nu}_e) = 4.9 \times 10^{-16}$ GeV, $\Gamma(\bar{B} \rightarrow D'_2 e \bar{\nu}_e) = 1.8 \times 10^{-16}$ GeV, and $\Gamma(\bar{B} \rightarrow D_3^* e \bar{\nu}_e) = 4.5 \times 10^{-16}$ GeV. The branching ratios of \bar{B} to D -wave charmed mesons are listed in Tab. II. We have listed others' results for comparison if available. Our results are about 5 times greater than that in Ref. [21]. It's noticeable that our results for decays into D_2 and D'_2 are in the same order, while in the results of QCD sum rules [21] $\mathcal{B}(\bar{B} \rightarrow D_2)$ is about 25 times larger than $\mathcal{B}(\bar{B} \rightarrow D'_2)$. The branching ratios for semi-leptonic decays of \bar{B}_s into D_{s2} , D'_{s2} and D_{s3}^* are listed in Tab. III. Our results for \bar{B}_s to D -wave charm-strange mesons are also much larger than the results of QCD sum rules in Ref. [22].

The branching ratios for B_c to D -wave $\bar{D}_J^{(*)}$, $B_J^{(*)}$ and $B_{sJ}^{(*)}$ are listed in Tab. IV. The branching ratios for semi-leptonic decays of B_c^- to \bar{D}_2 and \bar{D}_3^* are in the order of 10^{-5} , and for $B_c^- \rightarrow D'_2$ the results are in the order of 10^{-6} . These results are about 100 times smaller than that for $\bar{B}_{(s)}$ decays owing to the different CKM matrix elements. For D -wave bottom mesons, the semi-taunic mode is not available and for D -wave bottom-strange mesons, both the μ and τ modes are unavailable since the constraints of phase space. The branching ratios for $B_c^+ \rightarrow B_J^{(*)}$ are less than 10^{-8} and that for $B_c^+ \rightarrow B_{sJ}^{(*)}$ are less than 10^{-9} . The tiny branching fractions for B_c to D -wave bottomed mesons mainly due to the tiny phase space. Based on our results, the possibilities for the D -wave bottomed mesons to be detected in B_c decays are quite small by current experiments.

Table II: Branching ratios of \bar{B} semi-leptonic decays with $\tau_{\bar{B}} = 1.519 \times 10^{-12}$ s.

(10^{-4})					
Channels	Ours	Ref. [21]	Ref. [20]	Ref. [23]	Ref. [24]
$\bar{B} \rightarrow D_2 e \bar{\nu}$	11	1.5	0.1	-	-
$\bar{B} \rightarrow D_2 \mu \bar{\nu}$	11	1.5	0.1	-	-
$\bar{B} \rightarrow D_2 \tau \bar{\nu}$	0.080	-	-	-	-
$\bar{B} \rightarrow D'_2 e \bar{\nu}$	4.1	0.06	-	0.02	0.6
$\bar{B} \rightarrow D'_2 \mu \bar{\nu}$	4.1	0.06	-	0.02	-
$\bar{B} \rightarrow D'_2 \tau \bar{\nu}$	0.027	-	-	-	-
$\bar{B} \rightarrow D_3^* e \bar{\nu}$	10	2.1	0.1	-	-
$\bar{B} \rightarrow D_3^* \mu \bar{\nu}$	10	2.1	0.1	-	-
$\bar{B} \rightarrow D_3^* \tau \bar{\nu}$	0.054	-	-	-	-

Table III: Branching ratios of \bar{B}_s semi-leptonic decays with $\tau_{\bar{B}_s} = 1.512 \times 10^{-12}$ s.

Channels	Ours	Ref. [22]
$\bar{B}_s \rightarrow D_{s2} e \bar{\nu}$	1.7×10^{-3}	1.02×10^{-4}
$\bar{B}_s \rightarrow D_{s2} \mu \bar{\nu}$	1.7×10^{-3}	1.02×10^{-4}
$\bar{B}_s \rightarrow D_{s2} \tau \bar{\nu}$	1.4×10^{-5}	-
$\bar{B}_s \rightarrow D'_{s2} e \bar{\nu}$	5.2×10^{-4}	3.4×10^{-7}
$\bar{B}_s \rightarrow D'_{s2} \mu \bar{\nu}$	5.1×10^{-4}	3.4×10^{-7}
$\bar{B}_s \rightarrow D'_{s2} \tau \bar{\nu}$	3.4×10^{-6}	-
$\bar{B}_s \rightarrow D_{s3}^* e \bar{\nu}$	1.5×10^{-3}	3.46×10^{-4}
$\bar{B}_s \rightarrow D_{s3}^* \mu \bar{\nu}$	1.4×10^{-3}	3.46×10^{-4}
$\bar{B}_s \rightarrow D_{s3}^* \tau \bar{\nu}$	9.5×10^{-6}	-

The ratio $\mathcal{R}[D_J^{(*)}]$, defined as the ratio of semi-taunic branching ratio over semi-electronic branching ratios of decays $\bar{B} \rightarrow D_J^{(*)}$, namely, $\mathcal{R}[D_J^{(*)}] = \frac{\mathcal{B}[\bar{B} \rightarrow D_J^{(*)} \tau^- \bar{\nu}_\tau]}{\mathcal{B}[\bar{B} \rightarrow D_J^{(*)} e^- \bar{\nu}_e]}$, is sensitive to the new physics [25]. We present these ratios for decays to D -wave charmed mesons in Tab. V, from which we can see

Table IV: Semi-leptonic decay branching ratios of B_c to D -wave heavy-light mesons with $\tau_{\bar{B}_c} = 0.452 \times 10^{-12}$ s.

Channels	Br	Channels	Br	Channels	Br
$B_c^- \rightarrow \bar{D}_2 e \bar{\nu}$	2.2×10^{-5}	$B_c^- \rightarrow \bar{D}'_2 e \bar{\nu}$	4.0×10^{-6}	$B_c^- \rightarrow \bar{D}_3^* e \bar{\nu}$	1.2×10^{-5}
$B_c^- \rightarrow \bar{D}_2 \mu \bar{\nu}$	2.2×10^{-5}	$B_c^- \rightarrow \bar{D}'_2 \mu \bar{\nu}$	4.0×10^{-6}	$B_c^- \rightarrow \bar{D}_3^* \mu \bar{\nu}$	1.2×10^{-5}
$B_c^- \rightarrow \bar{D}_2 \tau \bar{\nu}$	7.7×10^{-6}	$B_c^- \rightarrow \bar{D}'_2 \tau \bar{\nu}$	1.2×10^{-6}	$B_c^- \rightarrow \bar{D}_3^* \tau \bar{\nu}$	3.1×10^{-6}
$B_c^+ \rightarrow B_2 e^+ \nu$	9.4×10^{-9}	$B_c^+ \rightarrow B'_2 e^+ \nu$	1.3×10^{-10}	$B_c^+ \rightarrow B_3^* e^+ \nu$	1.4×10^{-10}
$B_c^+ \rightarrow B_2 \mu^+ \nu$	1.7×10^{-9}	$B_c^+ \rightarrow B'_2 \mu^+ \nu$	7.6×10^{-12}	$B_c^+ \rightarrow B_3^* \mu^+ \nu$	2.0×10^{-11}
$B_c^+ \rightarrow B_{s2} e^+ \nu$	3.3×10^{-9}	$B_c^+ \rightarrow B'_{s2} e^+ \nu$	3.2×10^{-12}	$B_c^+ \rightarrow B_{s3}^* e^+ \nu$	5.6×10^{-13}

that, $\mathcal{R}[D_J^{(*)}]$ for \bar{B} decays and $\mathcal{R}[D_{sJ}^{(*)}]$ for \bar{B}_s decays, are almost the same and in the order of 10^{-3} , while $\mathcal{R}[\bar{D}_J^{(*)}]$ for B_c^- decays are in the order of 10^{-1} . This big difference is mainly due to the phase space. By simple integral over the phase space, we can find that, the phase space ratio of semi-tauonic decay to semi-electronic decay for B_c^- meson is about 30 times larger than that for \bar{B} or \bar{B}_s meson.

Table V: $\mathcal{R}[D_J^{(*)}] = \frac{\mathcal{B}[\bar{B} \rightarrow D_J^{(*)} \tau \bar{\nu}_\tau]}{\mathcal{B}[\bar{B} \rightarrow D_J^{(*)} e \bar{\nu}_e]}$, $\mathcal{R}[D_{sJ}^{(*)}] = \frac{\mathcal{B}[\bar{B}_s \rightarrow D_{sJ}^{(*)} \tau \bar{\nu}_\tau]}{\mathcal{B}[\bar{B}_s \rightarrow D_{sJ}^{(*)} e \bar{\nu}_e]}$, and $\mathcal{R}[\bar{D}_J^{(*)}] = \frac{\mathcal{B}[B_c^- \rightarrow \bar{D}_J^{(*)} \tau \bar{\nu}_\tau]}{\mathcal{B}[B_c^- \rightarrow \bar{D}_J^{(*)} e \bar{\nu}_e]}$, ratios of semi-tauonic branching ratio to semi-electronic branching ratio for \bar{B} , \bar{B}_s and B_c^- to D -wave charmed mesons.

Modes	D_2	D'_2	D_3^*	D_{s2}	D'_{s2}	D_{s3}^*	\bar{D}_2	\bar{D}'_2	\bar{D}_3^*
\mathcal{R}	0.0071	0.0065	0.0052	0.0079	0.0066	0.0064	0.35	0.29	0.25

The decay widths for $\bar{B}_{(s)}$ or B_c to 2^- states mesons are dependent on the mixing angle α , which can be showed by Fig. 6(a) and Fig. 6(b). This dependence for \bar{B} decays can be described by the following equations

$$\Gamma(\bar{B} \rightarrow D_2 e \bar{\nu}) = \Gamma_1 [1 + \lambda_1 \cos(2\alpha + \Theta_1)], \quad (29)$$

$$\Gamma(\bar{B} \rightarrow D'_2 e \bar{\nu}) = \Gamma_2 [1 - \lambda_2 \cos(2\alpha + \Theta_2)]. \quad (30)$$

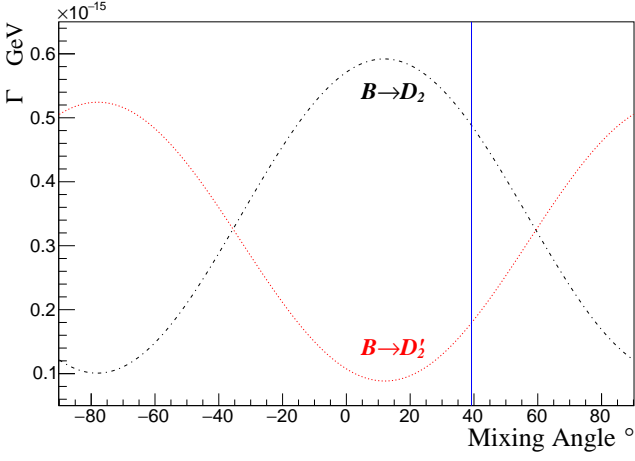
Our fit results give that the parameters are as

$$\begin{aligned} \Gamma_1 &= 3.46 \times 10^{-16}, & \lambda_1 &= 0.709, & \Theta_1 &= -23.7^\circ, \\ \Gamma_2 &= 3.06 \times 10^{-16}, & \lambda_2 &= 0.711, & \Theta_2 &= -24.1^\circ. \end{aligned}$$

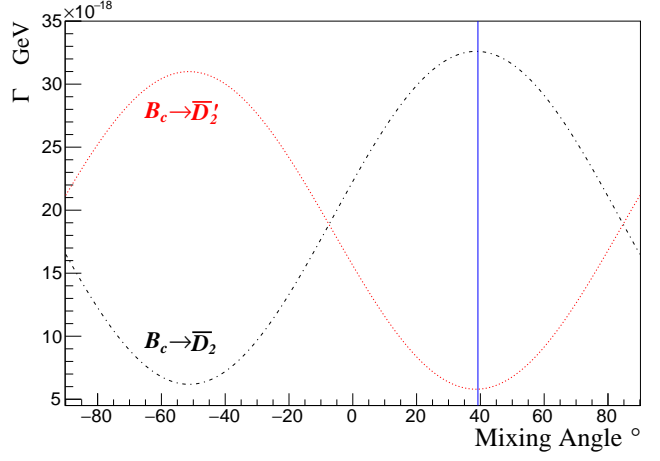
The tiny differences in parameters for D_2 and D'_2 come from the small difference between m_{D_2} and $m_{D'_2}$. In Fig. 6(c) and Fig. 6(d), we also show the ratios $\frac{\Gamma(\bar{B} \rightarrow D_2 e \bar{\nu})}{\Gamma(\bar{B} \rightarrow D'_2 e \bar{\nu})}$ and $\frac{\Gamma(B_c^- \rightarrow \bar{D}_2 e \bar{\nu})}{\Gamma(B_c^- \rightarrow \bar{D}'_2 e \bar{\nu})}$, which are very sensitive to the mixing angle.

4.3. Non-leptonic decay widths and branching ratios

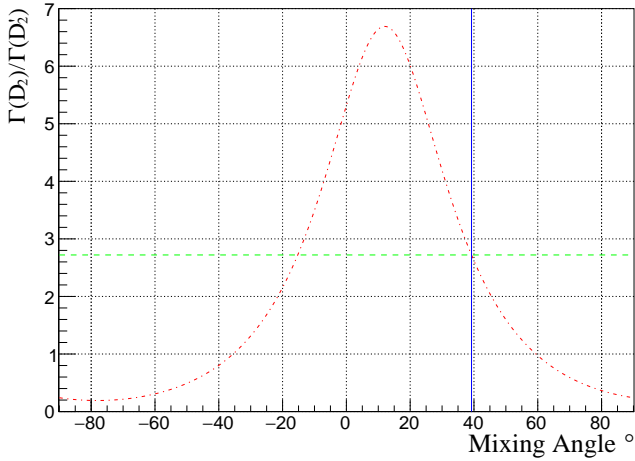
The non-leptonic decay widths are listed in Tab. VI, where we have kept the Wilson coefficient a_1 in order to facilitate comparison with other models. The corresponding branching ratios are listed in Tab. VII, where we have specified the values $a_1^b = 1.14$ for $b \rightarrow c(u)$ transition and $a_1^c = 1.2$ for $c \rightarrow d(s)$ transition. From the non-leptonic decay results we can see that, with the same final D meson, the ρ mode has the largest branching ratio and can reach 10^{-3} order in $\bar{B}_{(s)}$ decays, and 10^{-6} order in B_c decay. When the light mesons have the same quark constituents, the width for decay into vector meson (ρ, K^*) mode is about $2 \sim 3$ times greater than its pseudoscalar meson (π, K) mode.



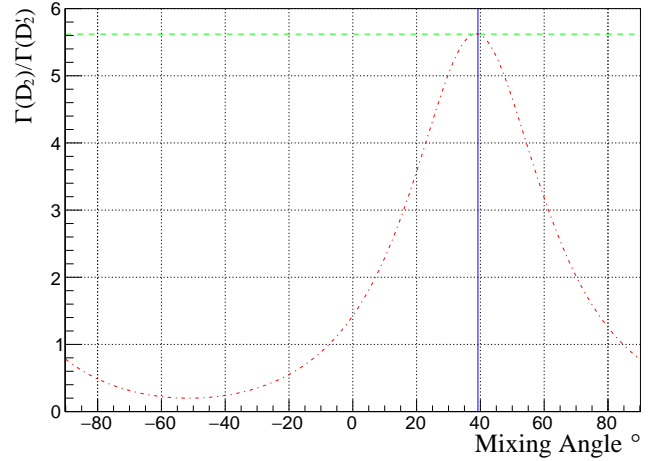
(a) $\bar{B} \rightarrow D_2^{(\prime)} e \bar{\nu}$ decay width vs mixing angle.



(b) $B_c^- \rightarrow \bar{D}_2^{(\prime)} e \bar{\nu}$ decay width vs mixing angle.



(c) $\Gamma(\bar{B} \rightarrow D_2 e \bar{\nu}) / \Gamma(\bar{B} \rightarrow D_2' e \bar{\nu})$ vs mixing angle.



(d) $\Gamma(B_c^- \rightarrow \bar{D}_2 e \bar{\nu}) / \Gamma(B_c^- \rightarrow \bar{D}_2' e \bar{\nu})$ vs mixing angle.

Fig. 6: Decay widths $\Gamma[\bar{B} \rightarrow D_2(D_2') e \bar{\nu}]$ and $\Gamma[B_c^- \rightarrow \bar{D}_2(\bar{D}_2') e \bar{\nu}]$ vary along with the mixing angle. The vertical solid line shows the results when mixing angle $\alpha = 39.23^\circ$, where the decay width ratio is 2.73 for $\bar{B} \rightarrow D_2(D_2') e \bar{\nu}$ and 5.63 for $B_c^- \rightarrow \bar{D}_2(\bar{D}_2') e \bar{\nu}$.

5. Summary

In this work we calculated semi-leptonic and non-leptonic decays of $\bar{B}_{(s)}$ into D -wave charmed mesons ($D_{(s)2}$, $D'_{(s)2}$, $D_{(s)3}^*$) and B_c into D -wave charmed and bottomed excited mesons. Form factors of hadronic transition are calculated by instantaneous Bethe-Salpeter methods. The semi-electronic branching ratios for $\bar{B}_{(s)} \rightarrow D_{(s)J}^{(*)}$ we got are about 10^{-3} order, and for B_c to D -wave charmed mesons are about 10^{-5} order. The non-leptonic branching ratios for decays to ρ mode can reach 10^{-3} order for $\bar{B}_{(s)}$ decays. So the D -wave D and D_s mesons are hopefully to be detected in $\bar{B}_{(s)}$ decays by current experiments. Our results reveal the branching fractions for B_c to D -wave bottomed mesons are less than 10^{-8} , which makes the D -wave bottomed mesons almost impossible to be discovered in B_c decays by current experiments.

We also present the angular distribution and charged lepton spectra for \bar{B} and B_c decays. The 2^- states D_2 and D_2' are the mixing states of $^1D_2 - ^3D_2$, so we present the dependence of the decay width varying along with the mixing angle. Based on our results, the semi-leptonic and non-leptonic branching ratios for $\bar{B}_{(s)}$ decays to the D -wave charm and charm-strange mesons have reached the experimental detection thresholds. These results would be helpful in future detecting and understanding these new D -wave excited $D_{(s)}$ mesons.

Table VI: Non-leptonic decay widths of \bar{B} , \bar{B}_s and B_c to D -wave heavy-light meson with general Wilson coefficient a_1 .

(GeV)					
Channels	Width	Channels	Width	Channels	Width
$\bar{B} \rightarrow D_2 \pi^-$	$2.8 \times 10^{-16} a_1^2$	$\bar{B} \rightarrow D'_2 \pi^-$	$9.8 \times 10^{-17} a_1^2$	$\bar{B} \rightarrow D_3^* \pi^-$	$2.2 \times 10^{-16} a_1^2$
$\bar{B} \rightarrow D_2 K^-$	$2.0 \times 10^{-17} a_1^2$	$\bar{B} \rightarrow D'_2 K^-$	$6.7 \times 10^{-18} a_1^2$	$\bar{B} \rightarrow D_3^* K^-$	$1.4 \times 10^{-17} a_1^2$
$\bar{B} \rightarrow D_2 \rho^-$	$5.5 \times 10^{-16} a_1^2$	$\bar{B} \rightarrow D'_2 \rho^-$	$2.0 \times 10^{-16} a_1^2$	$\bar{B} \rightarrow D_3^* \rho^-$	$4.7 \times 10^{-16} a_1^2$
$\bar{B} \rightarrow D_2 K^{*-}$	$2.9 \times 10^{-17} a_1^2$	$\bar{B} \rightarrow D'_2 K^{*-}$	$1.0 \times 10^{-17} a_1^2$	$\bar{B} \rightarrow D_3^* K^{*-}$	$2.5 \times 10^{-17} a_1^2$
$\bar{B}_s \rightarrow D_{s2} \pi^-$	$4.0 \times 10^{-16} a_1^2$	$\bar{B}_s \rightarrow D'_{s2} \pi^-$	$1.2 \times 10^{-16} a_1^2$	$\bar{B}_s \rightarrow D_{s3}^* \pi^-$	$2.9 \times 10^{-16} a_1^2$
$\bar{B}_s \rightarrow D_{s2} K^-$	$2.8 \times 10^{-17} a_1^2$	$\bar{B}_s \rightarrow D'_{s2} K^-$	$8.2 \times 10^{-18} a_1^2$	$\bar{B}_s \rightarrow D_{s3}^* K^-$	$1.9 \times 10^{-17} a_1^2$
$\bar{B}_s \rightarrow D_{s2} \rho^-$	$8.1 \times 10^{-16} a_1^2$	$\bar{B}_s \rightarrow D'_{s2} \rho^-$	$2.4 \times 10^{-16} a_1^2$	$\bar{B}_s \rightarrow D_{s3}^* \rho^-$	$6.4 \times 10^{-16} a_1^2$
$\bar{B}_s \rightarrow D_{s2} K^{*-}$	$4.2 \times 10^{-17} a_1^2$	$\bar{B}_s \rightarrow D'_{s2} K^{*-}$	$1.3 \times 10^{-17} a_1^2$	$\bar{B}_s \rightarrow D_{s3}^* K^{*-}$	$3.4 \times 10^{-17} a_1^2$
$B_c^- \rightarrow \bar{D}_2 \pi^-$	$1.5 \times 10^{-18} a_1^2$	$B_c^- \rightarrow \bar{D}'_2 \pi^-$	$3.2 \times 10^{-19} a_1^2$	$B_c^- \rightarrow \bar{D}_3^* \pi^-$	$1.4 \times 10^{-18} a_1^2$
$B_c^- \rightarrow \bar{D}_2 K^-$	$1.2 \times 10^{-19} a_1^2$	$B_c^- \rightarrow \bar{D}'_2 K^-$	$2.5 \times 10^{-20} a_1^2$	$B_c^- \rightarrow \bar{D}_3^* K^-$	$1.1 \times 10^{-19} a_1^2$
$B_c^- \rightarrow \bar{D}_2 \rho^-$	$4.5 \times 10^{-18} a_1^2$	$B_c^- \rightarrow \bar{D}'_2 \rho^-$	$1.0 \times 10^{-18} a_1^2$	$B_c^- \rightarrow \bar{D}_3^* \rho^-$	$4.1 \times 10^{-18} a_1^2$
$B_c^- \rightarrow \bar{D}_2 K^{*-}$	$2.7 \times 10^{-19} a_1^2$	$B_c^- \rightarrow \bar{D}'_2 K^{*-}$	$6.1 \times 10^{-20} a_1^2$	$B_c^- \rightarrow \bar{D}_3^* K^{*-}$	$2.4 \times 10^{-19} a_1^2$
$B_c^+ \rightarrow B_2 \pi^+$	$1.4 \times 10^{-19} a_1^2$	$B_c^+ \rightarrow B'_2 \pi^+$	$1.3 \times 10^{-21} a_1^2$	$B_c^+ \rightarrow B_3^* \pi^+$	$1.9 \times 10^{-21} a_1^2$

Acknowledgments

This work was supported in part by the National Natural Science Foundation of China (NSFC) under Grant Nos. 11405037, 11575048 and 11505039, and in part by PIRS of HIT Nos. T201405, A201409, and B201506.

A. Expressions for N_i s in the Hadronic Tensor $H_{\mu\nu}$

The hadronic tensor N_i ($i = 1, 2, 4, 5, 6$) for \bar{B} to D_2 meson are

$$N_1 = \frac{2M^4 \mathbf{p}_F^4 s_1^2}{3M_F^4} - \frac{4M^2 \mathbf{p}_F^2 s_1 s_3}{3M_F^2} - \frac{1}{2} M^2 \mathbf{p}_F^2 s_4^2 + \frac{s_3^2}{6}, \quad (\text{A.1})$$

$$N_2 = \frac{2E_F M^3 \mathbf{p}_F^2 s_1 s_3}{3M_F^4} + \frac{E_F M^3 \mathbf{p}_F^2 s_4^2}{2M_F^2} - \frac{E_F M s_3^2}{6M_F^2} + \frac{2M^4 \mathbf{p}_F^4 s_1 s_2}{3M_F^4} - \frac{2M^2 \mathbf{p}_F^2 s_2 s_3}{3M_F^2}, \quad (\text{A.2})$$

$$N_4 = \frac{4E_F M^3 \mathbf{p}_F^2 s_2 s_3}{3M_F^4} + \frac{2M^4 \mathbf{p}_F^4 s_2^2}{3M_F^4} - \frac{M^4 \mathbf{p}_F^2 s_4^2}{2M_F^2} + \frac{M^2 s_3^2 (M_F^2 + 4\mathbf{p}_F^2)}{6M_F^4}, \quad (\text{A.3})$$

$$N_5 = -\frac{M^4 \mathbf{p}_F^4 s_4^2}{2M_F^2} - \frac{M^2 \mathbf{p}_F^2 s_3^2}{2M_F^2}, \quad (\text{A.4})$$

$$N_6 = -\frac{M^2 \mathbf{p}_F^2 s_3 s_4}{M_F^2}. \quad (\text{A.5})$$

Here \mathbf{p}_F denotes the three-momentum of final D systems and $E_F = \sqrt{M_F^2 + \mathbf{p}_F^2}$. For \bar{B} to D'_2 the relations between N_i and form factors t_k ($k = 1, 2, 3, 4$) have the same form with that for D_2 , just s_k are replaced with t_k . Both s_k and t_k are functions of q_\perp^2 .

Table VII: Branching ratios of non-leptonic decays for \bar{B} , \bar{B}_s and B_c to D -wave heavy-light mesons. $a_1^b = 1.14$ for b quark decay and $a_1^c = 1.2$ for c quark decay.

Channels	Br	Channels	Br	Channels	Br
$\bar{B} \rightarrow D_2 \pi^-$	8.5×10^{-4}	$\bar{B} \rightarrow D'_2 \pi^-$	2.9×10^{-4}	$\bar{B} \rightarrow D_3^* \pi^-$	6.5×10^{-4}
$\bar{B} \rightarrow D_2 K^-$	5.9×10^{-5}	$\bar{B} \rightarrow D'_2 K^-$	2.0×10^{-5}	$\bar{B} \rightarrow D_3^* K^-$	4.3×10^{-5}
$\bar{B} \rightarrow D_2 \rho^-$	1.7×10^{-3}	$\bar{B} \rightarrow D'_2 \rho^-$	5.9×10^{-4}	$\bar{B} \rightarrow D_3^* \rho^-$	1.4×10^{-3}
$\bar{B} \rightarrow D_2 K^{*-}$	8.6×10^{-5}	$\bar{B} \rightarrow D'_2 K^{*-}$	3.1×10^{-5}	$\bar{B} \rightarrow D_3^* K^{*-}$	7.5×10^{-5}
$\bar{B}_s \rightarrow D_{s2} \pi^-$	1.2×10^{-3}	$\bar{B}_s \rightarrow D'_{s2} \pi^-$	3.6×10^{-4}	$\bar{B}_s \rightarrow D_{s3}^* \pi^-$	8.5×10^{-4}
$\bar{B}_s \rightarrow D_{s2} K^-$	8.3×10^{-5}	$\bar{B}_s \rightarrow D'_{s2} K^-$	2.5×10^{-5}	$\bar{B}_s \rightarrow D_{s3}^* K^-$	5.7×10^{-5}
$\bar{B}_s \rightarrow D_{s2} \rho^-$	2.4×10^{-3}	$\bar{B}_s \rightarrow D'_{s2} \rho^-$	7.3×10^{-4}	$\bar{B}_s \rightarrow D_{s3}^* \rho^-$	1.9×10^{-3}
$\bar{B}_s \rightarrow D_{s2} K^{*-}$	1.3×10^{-4}	$\bar{B}_s \rightarrow D'_{s2} K^{*-}$	3.8×10^{-5}	$\bar{B}_s \rightarrow D_{s3}^* K^{*-}$	1.0×10^{-4}
$B_c^- \rightarrow \bar{D}_2 \pi^-$	1.0×10^{-6}	$B_c^- \rightarrow \bar{D}'_2 \pi^-$	2.2×10^{-7}	$B_c^- \rightarrow \bar{D}_3^* \pi^-$	9.6×10^{-7}
$B_c^- \rightarrow \bar{D}_2 K^-$	8.0×10^{-8}	$B_c^- \rightarrow \bar{D}'_2 K^-$	1.7×10^{-8}	$B_c^- \rightarrow \bar{D}_3^* K^-$	7.5×10^{-8}
$B_c^- \rightarrow \bar{D}_2 \rho^-$	3.1×10^{-6}	$B_c^- \rightarrow \bar{D}'_2 \rho^-$	6.9×10^{-7}	$B_c^- \rightarrow \bar{D}_3^* \rho^-$	2.8×10^{-6}
$B_c^- \rightarrow \bar{D}_2 K^{*-}$	1.9×10^{-7}	$B_c^- \rightarrow \bar{D}'_2 K^{*-}$	4.2×10^{-8}	$B_c^- \rightarrow \bar{D}_3^* K^{*-}$	1.7×10^{-7}
$B_c^+ \rightarrow B_2 \pi^+$	1.4×10^{-7}	$B_c^+ \rightarrow B'_2 \pi^+$	1.3×10^{-9}	$B_c^+ \rightarrow B_3^* \pi^+$	1.9×10^{-9}

The hadronic tensor N_i for \bar{B} to D_3^* are expressed with form factors h_k ($k = 1, 2, 3, 4$) as

$$N_1 = \frac{2M^6 \mathbf{p}_F^6 h_1^2}{5M_F^6} - \frac{4M^4 \mathbf{p}_F^4 h_1 h_3}{5M_F^4} - \frac{4M^4 \mathbf{p}_F^4 h_4^2}{15M_F^2} + \frac{2M^2 \mathbf{p}_F^2 h_3^2}{15M_F^2}, \quad (\text{A.6})$$

$$N_2 = \frac{2E_F M^5 \mathbf{p}_F^4 h_1 h_3}{5M_F^6} + \frac{4E_F M^5 \mathbf{p}_F^4 h_4^2}{15M_F^4} - \frac{2E_F M^3 \mathbf{p}_F^2 h_3^2}{15M_F^4} + \frac{2M^6 \mathbf{p}_F^6 h_1 h_2}{5M_F^6} - \frac{2M^4 \mathbf{p}_F^4 h_2 h_3}{5M_F^4}, \quad (\text{A.7})$$

$$N_4 = \frac{4E_F M^5 \mathbf{p}_F^4 h_2 h_3}{5M_F^6} + \frac{2M^6 \mathbf{p}_F^6 h_2^2}{5M_F^6} - \frac{4M^6 \mathbf{p}_F^4 h_4^2}{15M_F^4} + \frac{2M^4 \mathbf{p}_F^2 h_3^2 (M_F^2 + 3\mathbf{p}_F^2)}{15M_F^6}, \quad (\text{A.8})$$

$$N_5 = -\frac{4M^6 \mathbf{p}_F^6 h_4^2}{15M_F^4} - \frac{4M^4 \mathbf{p}_F^4 h_3^2}{15M_F^4}, \quad (\text{A.9})$$

$$N_6 = -\frac{8M^4 \mathbf{p}_F^4 h_3 h_4}{15M_F^4}. \quad (\text{A.10})$$

B. Full Salpeter equations and the numerical solutions

B.1. Salpeter equations

Salpeter wave function $\varphi(q_\perp)$ is related to BS wave function $\Psi(q)$ by the following definition

$$\varphi(q_\perp) = i \int \frac{dq_P}{2\pi} \Psi(q), \quad \eta(q_\perp) = \int \frac{d^3 k_\perp}{(2\pi)^3} \varphi(k_\perp) V(|q_\perp - k_\perp|), \quad (\text{B.1})$$

where the 3-dimensional integration $\eta(q_\perp)$ can be understood as the BS vertex for bound states, and $V(|q_\perp - k_\perp|)$ denotes the instantaneous interaction kernel.

The projection operators $\Lambda_i^\pm(q_\perp)$ ($i = 1$ for quark and 2 for anti-quark) are defined as

$$\Lambda_i^\pm = \frac{1}{2\omega_i} \left[\frac{\not{P}}{M} \omega_i \pm (-1)^{i+1} (m_i + \not{q}_\perp) \right]. \quad (\text{B.2})$$

Then we define four wave functions $\varphi^{\pm\pm}$ by φ and Λ_i^\pm as

$$\varphi^{\pm\pm} \equiv \Lambda_1^\pm(q_\perp) \frac{\not{P}}{M} \varphi(q_\perp) \frac{\not{P}}{M} \Lambda_2^\pm(q_\perp), \quad (\text{B.3})$$

where φ^{++} and φ^{--} are called the positive and negative Salpeter wave function, respectively. And we can easily check that $\varphi = \varphi^{++} + \varphi^{+-} + \varphi^{-+} + \varphi^{--}$.

The full coupled Salpeter equations then can be expressed as [26]

$$\varphi^{+-} = \varphi^{-+} = 0, \quad (\text{B.4})$$

$$(M - \omega_1 - \omega_2)\varphi^{++} = +\Lambda_1^+(q_\perp)\eta(q_\perp)\Lambda_2^+(q_\perp), \quad (\text{B.5})$$

$$(M + \omega_1 + \omega_2)\varphi^{--} = -\Lambda_1^-(q_\perp)\eta(q_\perp)\Lambda_2^-(q_\perp). \quad (\text{B.6})$$

From above equations, we can see that in the weak binding condition $M \sim (\omega_1 + \omega_2)$, φ^{--} is much smaller compared with φ^{++} and can be ignored in the calculations. The normalization condition for Salpeter wave function reads

$$\int \frac{d^3 q_\perp}{(2\pi)^3} \left[\bar{\varphi}^{++} \frac{\not{P}}{M} \varphi^{++} \frac{\not{P}}{M} - \bar{\varphi}^{--} \frac{\not{P}}{M} \varphi^{--} \frac{\not{P}}{M} \right] = 2M. \quad (\text{B.7})$$

B.2. Numerical solutions of 0^- state

Now we take the 0^- (1S_0) state as an example to show the details of achieving Salpeter equations' numerical results. The Salpeter wave function for 0^- (1S_0) state has the following general form [44]

$$\varphi(^1S_0) = M \left[k_1 \frac{\not{P}}{M} + k_2 + k_3 \frac{\not{q}_\perp}{M} + k_4 \frac{\not{P}\not{q}_\perp}{M^2} \right] \gamma^5. \quad (\text{B.8})$$

By utilizing the Eq. (B.4), we have the following two constraint conditions

$$k_3 = \frac{M(\omega_1 - \omega_2)}{m_1\omega_2 + m_2\omega_1} k_2, \quad k_4 = -\frac{M(\omega_1 + \omega_2)}{m_1\omega_2 + m_2\omega_1} k_1. \quad (\text{B.9})$$

In above wave function, the only undetermined wave functions are k_1 and k_2 , which are the functions of q_\perp^2 .

By using the definition Eq. (B.3), we can easily get the positive Salpeter wave function of 1S_0 state as Eq. (17), and the corresponding constraint conditions Eq. (18). Similarly, the Salpeter negative wave function $\varphi^{--} (^1S_0)$ is expressed as

$$\varphi^{--} (^1S_0) = \left[Z_1 + Z_2 \frac{\not{P}}{M} + Z_3 \frac{\not{q}_\perp}{M} + Z_4 \frac{\not{P}\not{q}_\perp}{M^2} \right] \gamma^5. \quad (\text{B.10})$$

Z_i ($i = 1, 2, 3, 4$) has the following forms

$$\begin{aligned} Z_1 &= \frac{M}{2} \left[k_2 - \frac{\omega_1 + \omega_2}{m_1 + m_2} k_1 \right], & Z_3 &= -\frac{M(\omega_1 - \omega_2)}{m_1\omega_2 + m_2\omega_1} Z_1, \\ Z_2 &= \frac{M}{2} \left[k_1 - \frac{m_1 + m_2}{\omega_1 + \omega_2} k_2 \right], & Z_4 &= +\frac{M(m_1 + m_2)}{m_1\omega_2 + m_2\omega_1} Z_1. \end{aligned} \quad (\text{B.11})$$

And now the normalization condition Eq. (B.7) becomes

$$\int \frac{d^3 \mathbf{q}}{(2\pi)^3} \frac{8M\omega_1\omega_2 k_1 k_2}{(m_1\omega_2 + m_2\omega_1)} = 1. \quad (\text{B.12})$$

Inserting the Salpeter positive wave function Eq. (17), and negative wave function Eq. (B.10)

into Salpeter equations Eq. (B.5) and (B.6) respectively, we can obtain two coupled eigen equations on k_1 and k_2 [44] as

$$\begin{cases} (M - \omega_1 - \omega_2) [ck_1(\mathbf{q}) + k_2(\mathbf{q})] = \frac{1}{2\omega_1\omega_2} \int d^3\mathbf{k} [\beta_1 k_1(\mathbf{k}) + \beta_2 k_2(\mathbf{k})], \\ (M + \omega_1 + \omega_2) [k_2(\mathbf{q}) - ck_1(\mathbf{q})] = \frac{1}{2\omega_1\omega_2} \int d^3\mathbf{k} [\beta_1 k_1(\mathbf{k}) - \beta_2 k_2(\mathbf{k})], \end{cases} \quad (\text{B.13})$$

where we have used definition $c = \frac{\omega_1 + \omega_2}{m_1 + m_2}$ and the shorthand

$$\begin{aligned} \beta_1 &= \mathbf{k} \cdot \mathbf{q} (V_s + V_v) \frac{(\nu_1 + \nu_2)(\omega_1 + \omega_2)}{m_1\nu_2 + m_2\nu_1} - (V_s - V_v)(m_1\omega_2 + m_2\omega_1), \\ \beta_2 &= \mathbf{k} \cdot \mathbf{q} (V_s + V_v) \frac{(\nu_1 - \nu_2)(m_1 - m_2)}{m_1\nu_2 + m_2\nu_1} - (V_s - V_v)(m_1m_2 + \omega_1\omega_2 + \mathbf{q}^2). \end{aligned} \quad (\text{B.14})$$

In above equations, V_s and V_v are the scalar and vector parts defined in Cornell potential (see Eq. 28) respectively; we have used the definition $\nu_i = \sqrt{m_i^2 + \mathbf{k}^2}$ ($i = 1, 2$).

Then by solving the two coupled eigen equations numerically, we achieve the mass spectrum and corresponding wave functions k_1 , k_2 . Repeating the similar procedures we can obtain the numerical wave functions for 1D_2 , 3D_2 and 3D_3 states. Interested reader can see more details on solving the full Salpeter equations in Refs. [29, 44, 45].

C. Positive Salpeter wave function for 1S_0 , 1D_2 and 3D_2

The positive Salpeter wave function and its constraint conditions for 1D_2 state [35] are displayed in C.1 and C.2. And the undetermined wave function are f_1 and f_2 .

$$\psi_D(^1D_2) = e_{\mu\nu} q'_\perp{}^\mu q'_\perp{}^\nu \left[b_1 + b_2 \frac{\not{P}_F}{M_F} + b_3 \frac{\not{q}'_\perp}{M_F} + b_4 \frac{\not{P}_F \not{q}'_\perp}{M_F^2} \right] \gamma^5, \quad (\text{C.1})$$

$$\begin{aligned} b_1 &= \frac{1}{2} \left[f_1 + \frac{\omega'_1 + \omega'_2}{m'_1 + m'_2} f_2 \right], & b_3 &= - \frac{M_F(\omega'_1 - \omega'_2)}{m'_1\omega'_2 + m'_2\omega'_1} b_1, \\ b_2 &= \frac{1}{2} \left[f_2 + \frac{m'_1 + m'_2}{\omega'_1 + \omega'_2} f_1 \right], & b_4 &= - \frac{M_F(m'_1 + m'_2)}{m'_1\omega'_2 + m'_2\omega'_1} b_1. \end{aligned} \quad (\text{C.2})$$

The positive Salpeter wave function of 3D_2 state [45] and constraint conditions can be written as

$$\psi_D(^3D_2) = i\epsilon_{\mu\nu\alpha\beta} \frac{P_F^\nu}{M_F} q'^\alpha_\perp e^{\beta\delta} q'_\perp{}^\delta \gamma^\mu \left[i_1 + i_2 \frac{\not{P}_F}{M_F} + i_3 \frac{\not{q}'_\perp}{M_F} + i_4 \frac{\not{P}_F \not{q}'_\perp}{M_F^2} \right]. \quad (\text{C.3})$$

$$\begin{aligned} i_1 &= \frac{1}{2} \left[v_1 - \frac{\omega'_1 + \omega'_2}{m'_1 + m'_2} v_2 \right], & i_3 &= + \frac{M_F(\omega'_1 - \omega'_2)}{m'_1\omega'_2 + m'_2\omega'_1} i_1, \\ i_2 &= \frac{1}{2} \left[v_2 - \frac{m'_1 + m'_2}{\omega'_1 + \omega'_2} v_1 \right], & i_4 &= - \frac{M_F(m'_1 + m'_2)}{m'_1\omega'_2 + m'_2\omega'_1} i_1. \end{aligned} \quad (\text{C.4})$$

Here we also only have two undetermined wave function v_1 and v_2 .

In above equations C.1 ~ C.4 the indeterminate wave functions, such as f_1 and f_2 in $\psi_D(^1D_2)$, v_1 and v_2 in $\psi_D(^3D_2)$, which are functions of q'^2_\perp and can be determined numerically by solving the coupled Salpeter eigen equations B.5 and B.6.

References

References

- [1] P. del Amo Sanchez *et al.* (BABAR Collaboration), [Phys. Rev. D. **82**, 111101 \(2010\)](#).

- [2] R. Aaij *et al.* (LHCb Collaboration), [JHEP. **09**, 145 \(2013\).](#)
- [3] R. Aaij *et al.* (LHCb Collaboration), [Phys. Rev. D **90**, 072003 \(2014\).](#)
- [4] R. Aaij *et al.* (LHCb Collaboration), [Phys. Rev. D **91**, 092002 \(2015\).](#)
- [5] R. Aaij *et al.* (LHCb Collaboration), [Phys. Rev. D **92**, 032002 \(2015\).](#)
- [6] S. Godfrey and N. Isgur, [Phys. Rev. D **32**, 189 \(1985\).](#)
- [7] B. Aubert *et al.* (BABAR Collaboration), [Phys. Rev. Lett.**97**, 222001 \(2006\).](#)
- [8] B. Aubert *et al.* (BABAR Collaboration), [Phys. Rev. D **80**, 092003 \(2009\).](#)
- [9] R. Aaij *et al.* (LHCb Collaboration), [Phys. Rev. Lett. **113**, 162001 \(2014\).](#)
- [10] R. Aaij *et al.* (LHCb Collaboration), [Phys. Rev. D **90**, 072003 \(2014\).](#)
- [11] Xian-Hui Zhong, [Phys. Rev. D **82**, 114014 \(2010\).](#)
- [12] Zhi-Feng Sun, Jie-Sheng Yu, Xiang Liu, and T. Matsuki, [Phys. Rev. D **82**, 111501 \(2010\).](#)
- [13] B. Chen, L. Yuan, and A. Zhang, [Phys. Rev. D **83**, 114025 \(2011\).](#)
- [14] Zhi-Gang Wang, [Phys. Rev. D **83**, 014009 \(2011\).](#)
- [15] Qi-Fang Lü and De-Min Li, [Phys. Rev. D **90**, 054024 \(2014\).](#)
- [16] B. Chen, X. Liu, and A. Zhang, [Phys. Rev. D **92**, 034005 \(2015\).](#)
- [17] Guo-Liang Yu, Zhi-Gang Wang, and Zhen-Yu Li, [Chin. Phys. C **39**, 063101 \(2015\).](#)
- [18] S. Godfrey and K. Moats, [Phys. Rev. D **90**, 117501 \(2014\).](#)
- [19] S. Godfrey and K. Moats, [Phys. Rev. D **93**, 034035 \(2016\).](#)
- [20] P. Colangelo, F. De Fazio, and G. Nardulli, [Phys. Lett. B **478**, 408 \(2000\).](#)
- [21] Long-Fei Gan and Ming-Qiu Huang, [Phys. Rev. D **79**, 034025 \(2009\).](#)
- [22] Long-Fei Gan *et al.*, [Eur. Phys. J. C **75**, 232 \(2015\).](#)
- [23] T.B. Suzuki, T. Ito, S. Sawada, and M. Matsuda, [Prog. Theor. Phys. **91**, 757 \(1994\).](#)
- [24] S. Veseli and M.G. Olsson, [Phys. Rev. D **54**, 886 \(1996\).](#)
- [25] J.P. Lees *et al.* (BaBar Collaboration), [Phys. Rev. Lett. **109**, 101802 \(2012\).](#)
- [26] E.E. Salpeter, [Phys. Rev. **87**, 328 \(1952\).](#)
- [27] E. Salpeter and H. Bethe, [Phys. Rev. **84**, 1232 \(1951\).](#)
- [28] Zhi-hui Wang, Guo-Li Wang, and Chao-Hsi Chang, [J. Phys. G: Nucl. Part. Phys. **39**, 015009 \(2012\).](#)
- [29] T. Wang, Guo-Li Wang, Y. Jiang, and Wan-Li Ju, [J. Phys. G. **40**, \(2013\) 035003.](#)
- [30] Wan-Li Ju, Guo-Li Wang, Hui-Feng Fu, Zhi-Hui Wang, and Ying Li, [JHEP **09**, 171 \(2015\).](#)
- [31] Q. Li, T. Wang, Y. Jiang, H. Yuan, and G.-L. Wang. [arXiv:1603.02013 \[hep-ph\].](#)
- [32] Guo-Li Wang, [Phys. Lett. B **633**, 492 \(2006\).](#)

- [33] Guo-Li Wang, [Phys. Lett. B **650**, 15 \(2007\)](#).
- [34] Guo-Li Wang, [Phys. Lett. B **674**, 172 \(2009\)](#).
- [35] Tianhong Wang, Guo-Li Wang, Wan-Li Ju, and Yue Jiang, [JHEP **03**, 110 \(2013\)](#).
- [36] D. Fakirov and B. Stech, [Nucl. Phys. B **133**, 315 \(1978\)](#).
- [37] N. Cabibbo and L. Maiani, [Phys. Lett. B **73**, 418 \(1978\)](#).
- [38] C.-H. Chang and Y.-Q. Chen, [Phys. Rev. D **49**, 3399 \(1994\)](#).
- [39] M. A. Ivanov, J. G. Körner, and P. Santorelli, [Phys. Rev. D **73**, 054024 \(2006\)](#).
- [40] E. Hernández, J. Nieves, and J. M. Verde-Velasco, [Phys. Rev. D **74**, 074008 \(2006\)](#).
- [41] R.N. Faustov and V.O. Galkin, [Phys. Rev. D. **87**, 034033 \(2013\)](#).
- [42] M. J. Dugan and B. Grinstein, [Phys. Lett. B **255**, 583 \(1991\)](#).
- [43] S. Mandelstam, [Proc. Roy. Soc. A **233**, 248 \(1955\)](#).
- [44] C.S. Kim and Guo-Li Wang, [Phys. Lett. B **584**, 285 \(2004\)](#).
- [45] T. Wang, H.-F. Fu, Y. Jiang, Q. Li, and G.-L. Wang, [arXiv:1601.01047 \[hep-ph\]](#).
- [46] L. Bergström, H. Grotch, and R.W. Robinett, [Phys. Rev. D. **43**, 7 \(1991\)](#).
- [47] T. Matsuki, T. Morii, and K. Seo, [Prog. Theo. Phys. **124**, 2 \(2010\)](#).
- [48] D. Ebert, R.N. Faustov, and V.O. Galkin, [Eur. Phys. J. C **66**, 197 \(2010\)](#).
- [49] K.A. Olive *et al.* (Particle Data Group), [Chin. Phys. C **38**, 090001 \(2014\)](#).
- [50] N. Devlani, V.H. Kher, and A.K. Rai, [EPJ. Web. Conf. **95**, 05006 \(2015\)](#).
- [51] N. Devlani and A.K. Rai, [Eur. Phys. J. A **48**, 104 \(2012\)](#).